Title
Impact of coupled heat transfer and water flow on soil borehole thermal energy storage (SBTES) systems: Experimental and modeling investigation

Authors
Moradi, Ali
Smits, Kathleen M
Massey, Jacob
et al.

Publication Date
2015-09-01

DOI
10.1016/j.geothermics.2015.05.007

Peer reviewed

Impact of Coupled Heat Transfer and Water Flow on Soil Borehole Thermal Energy Storage (SBTES) Systems: Experimental and Modeling Investigation

Ali Moradi[1*], Kathleen M. Smits[1], Jacob Massey[1], Abdullah Cihan[2], John McCartney[3]

[1]*Center for Experimental Study of Subsurface Environmental Processes (CESEP), Department of Civil and Environmental Engineering, Colorado School of Mines, Golden, CO, U.S.A.*

[2]*Earth Sciences Division, Lawrence Berkeley National Laboratory Berkeley, CA, U.S.A.*

[3]*Department of Civil and Environmental Engineering, University of Colorado, Boulder, CO, U.S.A.*

* *Corresponding Author:amoradig@mines.edu*

Abstract

A promising energy storage option is to inject and store heat generated from renewable energy sources in geothermal borehole arrays to form soil-borehole thermal energy storage (SBTES) systems. Although the method is gaining attention, there is no general agreement on the best numerical modeling approach to determine system effectiveness. Although it is widely recognized that the movement of water in liquid and vapor forms is closely coupled to heat transfer process, these coupled processes are often not considered in modeling of SBTES systems. Oftentimes, approaches assume that the soil is a purely conductive medium with constant hydraulic and thermal properties, which may affect SBTES system predictions. Numerical modeling tools that are available to consider these coupled processes, have not been applied to SBTES systems, partly due to the scarcity of field or laboratory data needed to validate these models. Thus, the need exists to systematically compare modeling efforts and experimental observations. The goal of this work is to test different conceptual and mathematical formulations that are used in heat and mass transfer theories and determine their importance to modeling SBTES systems. Such a comparison required the modification of a non-isothermal numerical model that simulates coupled heat, water vapor and liquid water flux through soil and considers non-equilibrium liquid/gas phase change. This model was used to investigate different processes (e.g. considering conduction and convection) and hydraulic and thermal parameterizations (e.g. considering temperature effect on saturation-capillary relation and thermal conductivity) on SBTES system behavior. Precision data under well controlled boundary conditions were generated and results from numerical simulations were compared to observations. Results demonstrate the need to include thermally induced moisture flow in modeling efforts as well as convective heat transfer, especially when modeling unsaturated flow systems. Convective heat flux arising from thermally induced moisture flow leads to greater heat transfer than to conductive flux alone. Comparisons of different formulation validate the need for further research for better modeling accuracy.

<u>Key words</u>: SBTES systems, Vadose zone, Convective heat transfer, Phase change, Numerical model, Experimental investigation

1 Introduction

The rapidly growing gap between consumption and production of energy associated with non-renewable energy sources can be addressed by introducing new cost-effective and clean energy sources such as wind or solar energy. An important issue limiting the implementation and use of renewable sources is energy storage as it is not possible to control the timing of the supply of solar or wind energy in spite of their abundance. For example, unlocking solar energy's full potential becomes relatively complex because its rate of generation is highest mid-day and during summer months, which is offset from the timing of the highest rates of consumption in winter (Pinel et al., 2011). Although a significant amount of research is being devoted to storage of electricity, the storage of heat can be more cost-effective and can be done on different scales. Soil-borehole thermal energy storage (SBTES) systems are one such technology that has been shown to be effective at storing heat collected by solar thermal panels in the summer and extracting it during the winter (Sibbitt et al., 2007; 2012). SBTES systems involve direct circulation of heated fluid through closed-loop geothermal heat exchangers in vertical borehole arrays (Pinel et al., 2011). The geothermal heat exchangers are typically designed with a closer spacing than in ground-source heat pump (GSHP) systems. The subsurface soil and rock provides an excellent medium for heat storage due to their relative abundance along with their relatively high specific heat capacities (Gabrielsson et al. 2000). The top or surface of a SBTES system typically includes a heat insulated cap to reduce thermal losses to the environment (Sibbitt et al., 2007; Pavlov and Olesen, 2012).

SBTES systems are attractive from an energy sustainability perspective for many reasons. They usually harvest their energy from renewable energy sources (solar-thermal), are low cost compared to other energy storage systems, and space efficient (i.e. underground) and therefore implementable in many locations (e.g. populated and rural environments). In addition, SBTES systems do not require long-distance energy transportation (localized energy storage), and are scalable from residential- to community- to utility-scale applications.

Although pilot programs are successfully utilizing SBTES systems (e.g., Sibbitt et al., 2007), two of the main limitations in large-scale implementation are low system efficiency and high initial installation costs (Hughes, 2008). Efficiency is usually defined as the ratio of the total heat extracted from the SBTES space during discharge or usage periods to the total heat injected into the SBTES space. In general, efficiency depends on the volume and geometry of the SBTES space, number, length and spacing of the boreholes, injection/withdrawal scheme, and mechanical, hydrological, and thermal properties of the soil/ rock (Ohga and Mikoda 2001). Zhang et al., (2012) numerically simulated heat transfer of a SBTES system at Drake Landing Solar Community (DLSC), Alberta, Canada. In their numerical model, they imposed time-dependent heat injection and withdrawal rates measured at the site but did not include variable soil thermal properties and water flow through unsaturated soil. They predicted an energy recovery efficiency of approximately 27% after 10 years. Despite the low efficiency, Sibbitt et al. (2007) found that the SBTES system at DLSC provided over 90% of the heat required for 52 single-family homes. However, Zhang et al. (2012) noted that in most SBTES implementations the parameters controlling the efficiency of the system have not been clearly delineated. Pavlov and Olesen (2012) mentioned that although seasonal storage plants are used in some countries (e.g. Germany, Sweden, Canada, etc.), the concept is not widely implemented due to the low efficiency versus initial cost. Increasing the efficiency of these systems will result in a decrease in installment and implementation costs, making the systems more attractive. However, central solar heating plants with seasonal storage require further research, specifically into the storage efficiency and how to best increase the efficiency.

An opportunity to enhance the efficiency of SBTES systems is to install them in the vadose zone (the unsaturated zone of soil above the water table) as proposed by McCartney et al. (2013). In this case, it is possible to take advantage of phase change and convective heat transfer phenomena in the pore water to obtain greater heat injection and extraction rates by formation of a convective cell between the borehole heat exchangers making the SBTES system more efficient. Convection can play a major role in transporting energy in unsaturated soils subject to a temperature gradient. For example, when the water around the heat exchanger array is heated, it can vaporize and move towards colder soil regions (i.e. away from the heat source). The water vapor then cools and condenses, releasing latent heat. Depending on the soil properties and initial moisture conditions, the liquid water can move due to the hydraulic gradient back toward the dry soil (i.e. towards the heat source) or accumulate.

Numerical modeling of ground heat exchangers can be performed either from the fluid within the U-tube to the borehole wall or from the surface of the borehole to the surrounding soil

(Shirazi and Bernier, 2013). In the first category, attention has been paid to modeling heat transfer processes through the fluid and grout inside and within the borehole with the aim of estimating the borehole's thermal resistance and the outlet fluid temperature (e.g. Hellstrom, 1991; Zeng et al., 2003; Diao et al., 2004). The grout consists of a mixture of silica sand and bentonite clay with some thermally-enhanced additives, and is used to backfill the borehole to assure maximum heat transfer between the heat exchanger and the borehole (Florides and Kalogirou, 2007). For heat transfer outside of the borehole (i.e. from the surface of the borehole to the surrounding soil), several analytical and numerical models have been proposed, for instance, Kelvin's line source model (Ingersoll and Plass, 1948), the cylindrical source model (Carslaw and Jaeger, 1946), the model of Eskilson (1987), and the finite line source model (Zeng et al., 2002). A few numerical studies are also available in the literature in which both fluid flow inside the borehole and heat transfer outside of the borehole are modeled (e.g. Rees and He, 2013). A detailed review of analytical and numerical models for analyzing the thermal behavior inside and outside of the U-tube can be found in the review paper presented by Yang et al. (2010) and Lamarche et al. (2010). It is important to note that none of these analytical models have incorporated coupled heat and mass transfer processes.

A common assumption in most SBTES numerical model approaches is to consider the soil as a purely conductive medium with constant hydraulic and thermal properties (Angelotti et al., 2014). Nonetheless, inlet fluid temperatures can create considerable temperature gradients and consequently moisture flow in regions surrounding the heat exchangers (Reuss et al., 1997). In soil science and hydrology literature, there are many experimental/numerical studies that investigate both heat and mass transfer simultaneously. As much understanding to SBTES can be gained from this literature, the next few paragraphs provide a brief review of some of the pertinent studies.

A large body of experimental observations is available on the movement of moisture under non-isothermal conditions (e.g., Bouyoucos, 1915; Smith, 1943; Taylor and Gavazza, 1954; Philip and de Vries, 1957). Bouyoucos (1915) demonstrated that in a soil column of uniform saturation, water flows from the warmer portion towards the colder portion. His finding was later confirmed in more detail by others (e.g., Smith, 1943; Maclean and Gwatkin 1946), who concluded that for each soil type, there is an optimum degree of saturation in which maximum transfer of water occurs. Several experimental studies have been conducted thereafter in developing hypotheses to describe the mechanisms of thermally induced moisture movement. Gurr et al. (1952) performed a series of experiments on a closed column of loam soil to assess the contribution of liquid water and water vapor flow due to temperature gradients. They showed that water vapor moves toward the colder regions in the soil, condenses, and returns to the warmer regions in the form of liquid water. They theoretically demonstrated that when sufficient moisture exists in the soil, equilibrium is not reached and water circulates continuously. After 1960, several papers were published which were mostly devoted to quantifying the importance of thermal gradients on moisture transfer rather than confirming the occurrence of the phenomena (e.g., Cary, 1965; Cassel et al., 1969; Bach, 1992). The purpose of most of these studies was to develop and evaluate the theoretical relationships, validated by experimental results.

There are a few works related to the uncertainties associated with hydraulic and thermal properties of the soil with application to GSHP systems. Based on the Philip and de Vries (1957) theory of heat and mass transfer, Reuss et al. (1997) developed a computer model to simulate combined heat and moisture transport for temperatures up to 90 °C. In their study, the model is validated using several laboratory and field scale experiments. They showed that thermal conductivity, heat capacity and overall thermal performance of seasonal heat storage systems highly depend on the soil degree of saturation. However, they did not show the overall importance of including these thermal properties under varying soil saturation conditions in modeling efforts. The study by Leong et al. (1998) showed that the degree of saturation has a crucial effect on performance of GHP systems. Their study suggested that a higher degree of saturation results in higher system efficiency, although variations in degrees of saturation above 50% has a relatively insignificant effect. Pavlov and Olesen (2012) discussed that thermal properties (e.g., heat capacity, thermal conductivity) of soil dictate spacing of boreholes that contain heat exchangers. However, they did not consider the effect of soil degree of saturation and temperature on soil thermal properties. Pinel et al. (2011) highlighted the effect of water diffusion or time/space variation of humidity on the performance of buried heat sources. They suggested that to account for the heat convection due to moisture transfer in the soil, a comprehensive model including both heat and mass transfer processes is required. What previous research demonstrates is that any experimental or theoretical study of SBTES systems behavior should involve both heat and mass transfer as well as non-isothermal conditions. In addition, the soil thermal and hydraulic properties should be defined as a function of environmental conditions.

One important property that needs to properly understand soil thermal performance is thermal conductivity which is subject to change in both space and time. Most models of SBTES assume that the thermal conductivity is constant although it is well known that it varies significantly with changes in saturation, temperature, soil density, grain size, porosity (η), mineral content, organic content, soil structure, and soil texture (e.g., Yadav and Saxena, 1977; Abu-Hamdeh, 2003). Several models have been proposed to estimate the thermal conductivity/soil degree of saturation relationship based on easily measurable soil parameters (e.g., de Vries, 1963; Johansen, 1975; Campbell, 1985; Campbell et al., 1994; Tarnawski et al., 2000), very few consider the influence of changes in temperature. Campbell et al. (1994) as well as Tarnawski et al. (2000) proposed models to predict thermal conductivity of soil as a function of temperature, soil moisture and composition of the porous media based on de Vries model (1957) and Johansen (1975) models, respectively. Overall, these studies highlight the need for considering the effect of temperature and soil moisture variability on soil thermal properties applicable to design and implement more efficient SBTES systems. Furthermore, as mentioned by She and Sleep (1998), the knowledge of temperature effect on capillary pressure-saturation relationship for multiphase fluid systems under non-isothermal conditions is necessary.

Based on the aforementioned studies, it is notable that although the assumption of constant ground hydraulic and thermal properties is valid for many cases (e.g. when completely dry or saturated conditions exist in the soil.), there is no clear definition of situations in which the effect of mass transfer in efficiency of seasonal heat storage systems can be neglected (Pinel et al., 2011). Most of previous studies were performed without consideration of high temperature gradients which is of critical importance for implementing SBTES systems (Reuss et al., 1997). Generally, the validation behind the physics governing the coupling of multiphase flow and heat transfer has not been implemented in both design and operation of SBTES systems to date. Consequently, developing new modeling techniques along with suitable experimental tools to add more complexity in defining the physics of the heat and mass transport has critical importance in obtaining necessary knowledge in efficient design and implementation of SBTES systems.

The goal of this paper is to better understand heat and mass transfer processes for SBTES systems installed in the vadose zone. We modified a fully coupled numerical model previously developed by Smits et al. (2011, 2012) that solves for heat, liquid water and water vapor flux and allows for non-equilibrium liquid/gas phase change. We then used this model to investigate the influence of different hydraulic and thermal parameterizations on system behavior as well as further examine the importance of considering convection and conduction in heat transfer for SBTES modeling efforts. To better understand the physical processes and test the numerical model formulation, we performed a series of two dimensional experiments. A two-dimensional, heated tank apparatus was designed, constructed and implemented with a series of sensors to monitor changes in temperature, volumetric water content and soil thermal properties. Four experiments were performed with different sands with varying grain size. The numerical model along with experimental results were used to test system behavior, perform a series of sensitivity analysis, and determine the importance of including/excluding certain processes from SBTES modeling efforts. Numerical modeling is aimed at better understanding of the physical processes within the system and illustrating any discrepancies between experimental and numerical results. The validated numerical model can also be used to simulate behavior of different soil types without conducting experiments. Although experimental test cases provide insight to coupled heat and moisture transfer, it is not possible to draw general conclusions with limited number of tests. Accordingly, validated numerical models are a good tool to investigate the effect of different parameters and processes on SBTES system efficiency.

2 Material and methods

In this section, a detailed review of the experiment apparatus and procedures along with a description of sand materials is presented. A review of governing equations of numerical model for the heat, liquid and water vapor transport is also provided.

2.1 Sand Material

Three types of uniform specialty silica sands (from Unimin Corp., Ottawa, MN) were used during experimentation. Identified by the effective sieve number, these include #12/20, #30/40, and #50/70 and a mixture of #12/20 and #50/70 sands. The mixing fraction for the 12/20 mixture was 70% 12/20 and 30% 50/70, herein referred to as C7F3. This mixing fraction was selected to ensure that the minimum porosity (i.e. maximum density) of the mixture was achieved; a minimum porosity can be achieved for mixtures containing 30% by volume of fine particles (i.e., C: F ratio of 7:3) as demonstrated by Koltermann and Gorelick (1995), and Sakaki and Smits 2014. The geotechnical and hydraulic properties of the different soils are presented in Table 1. The properties for Bonny silt is also included in the table, as the properties for this soil are used in the validated numerical model to evaluate the role of a soil having a wider grain size distribution and different water retention characteristics. All three sands have different mean diameter sizes but have similar porosities. The uniformity coefficient for the sands is approximately 1.2, the grain density is 2650 kg.m-3, the grain shape is rounded, and the dominating mineral composition is quartz (99.8%) (Accusands, Unimin Corps., Ottowa).

[Table 1 here]

The thermal conductivity-degree of saturation relationships and drainage-path water retention curves (WRC) measured at room temperature for the four sands are shown in Figure 1. These results were obtained using a modified Tempe cell that allowed continuous monitoring of water content, capillary pressure, temperature, and soil thermal properties. Details of experimental apparatus and procedures can be found in Smits et al. (2010, 2013). As seen from this figure, the apparent λ increases with decreasing degree of saturation. #12/20 and #30/40 sands have similar trends while λ values for the sand mixture (C7F3) are considerably higher than for the other uniform sands. In the sand mixture, the fine particles fill the void spaces between the coarse particles, increasing the contact between sand particles and in the case of the C7F3, decreasing the porosity. As a result, the overall thermal conductivity of the mixture increases. The shape of the WRC depends on the particle size distribution (or pore space distribution). For uniform sands, since the pore spaces are uniformly distributed, they drain simultaneously once the displacement pressure is reached, resulting in the flat shape of WRC. However, for the mixed sand case, mixing is not as ideal or uniform, and some pores are filled more with the fines and other are filled less. Under such conditions, the less or unfilled pores drain early but after the large pores drain, the suction continues to increase. The influence of the fine soil particles controls the behavior, and the resulting WRC is steeper than that of the unmixed soils.

[Figure 1 here]

2.2 Experimental Apparatus

Experiments were conducted using a two dimensional test tank with dimensions of 609.6 mm high, 609.6 m in depth, and 89 mm in width. The tank was formed from rectangular pieces of 12.7 mm-thick Plexiglas. Custom-made aluminum heat plates from ABM Fabrication & Machining of Arvada, CO were placed inside the tank on the left and right boundaries to serve as constant temperature sources. Within the aluminum plates, a U-shape flow channel was incorporated to permit flow of heated water from the heat plate's inlet port, through the flow channels inside the tank, and out of the outlet port. The inlet and outlet ports were located at the top of each heat plate and connected to tubing, providing constant temperature water from the circulator. Schematics of the 2D tank along with the sensor locations and plumbing details are shown in Figure 2.

At each inlet and outlet port, temperature was monitored using pipe plug thermocouples (RT-1, 2 cm probe length with 0.1 °C resolution, Decagon Devices Inc.) Heated fluid was supplied and pumped by a circulating bath machine with precise temperature control (Polyscience model AD07R-20). A total of 22 temperature (EC-T, 38 mm probe length, Decagon Devices Inc.) and 22 dielectric (ECH2O EC-5, 55-mm prong length, 70-MHz measurement frequency, Decagon Devices Inc.) sensors were installed throughout the tank at the locations shown in Figure 2. Prior to experimentation, all EC-5 sensors were calibrated using the method developed by Sakaki et al. (2008) to account for sensor-to-sensor variability readings for the analog-to-digital converter counts. Em50 (Decagon, Inc.) data loggers with five sensor ports were used to read and log data. A thermal property analyzer (KD-2 Pro, Decagon Devices Inc.) connected to a 30 mm SH-1 dual needed heat pulse sensor was used to monitor changes in soil thermal properties 50 mm below the soil surface during the experiment. The SH-1 thermal sensor is a dual needle probe, where the needles are 30 mm in length and separated by a distance of 6 mm. In these sensors, Heat is applied in one needle in a set heating time followed by a cooling period. The temperature is measured in the monitoring needle and thermal properties of thermal conductivity (λ), volumetric heat capacity (C), and diffusivity (D) are then calculated based on the line heat source analysis.

To test the accuracy of moisture sensors, possible sources of error were considered. Air gaps between sensor rods and soil can be a source of error in sensor readings (Ruelle and Laurent, 2008). Air gaps can occur during installation or soil shrinkage due to drying (Hillel, 1998). One way to avoid these gaps is working with moist soil (Varble and Chávez, 2011).

Therefore, the tank was wet packed to eliminate this source of error. Furthermore, accuracy of EC-5 sensors can be influenced by temperature changes in the soil. This is due to change in dielectric transitivity of the bulk soil by temperature. As shown by Kizito et al. (2008), temperature sensitivity of EC-5 sensors can be corrected through data processing if the temperature of the soil is known in the same location. To evaluate the accuracy of temperature sensitivity correction method used in this study, a set of isothermal experiments were conducted. In these experiments, the moisture readings of the sensors were compared to the actual moisture values of the soil sample which were experimentally measured. Based on the results, it was found that temperature sensitivity up to 60°C is negligible for moisture sensors used in our experimentation. Five temperature sensors were placed outside of the experimental apparatus to monitor heat losses from the tank as well as ambient conditions.

Two constant head devices supplied by a constant water source through the use of a pump were connected to valves on either side of the tank (see Figure 2) and used to supply constant water head to the system. The constant head devices allowed us to maintain the water table at a predetermined level throughout the course of each experiment. Top and bottom sides of the tank were thermally insulated.

[Figure 2 here]

2.3 Experimental Procedure

Four experiments were performed as part of this study, as summarized in Table 1. For each experiment, the sand was carefully wet-packed with deionized water in 20-mm lifts using the procedure outlined by Sakaki and Illangasekare (2007). This method is used to assure that a homogenous soil sample is achieved. This packing method result in greater densities by the repeated tapping of the tank side walls following the procedures outlined in ASTM D 4253. An advantage of using this method instead of a vibratory device is that damage to the sensitive network of sensors in the 2D tank is minimized. After wet-packing the sand into the tank, the constant head device was adjusted to allow the soil sample drain to a predetermined water table level. Based on the air entry value of each sand type, the constant hydraulic head devices were adjusted to establish a water table such that the first row of sensors from bottom of the tank was located in the capillary fringe region. The purpose of this was to study the soil hydraulic and thermal behavior under both saturated and unsaturated conditions. After establishing the initial condition for degree of saturation distribution, the circulating heat bath machine was turned on to circulate the water through the heat plates on the left and right sides of the tank at a constant temperature of 60 °C. All tests were conducted for 7 days.

3 Experimental results and discussion

In this section, we present a demonstration of experimental results for all experiments. The discussion was mostly based on data from EX-2 with comparison to other experiments (EX-1, 3, and 4) where observed trends and differences between experiments are noted. It should be mentioned that in this paper, moisture flow is referred to both liquid water and water vapor flow in the system. The reason we show these results is to demonstrate the observed thermal and hydraulic behavior of different soils.

3.1 Temperature behavior in soil

The temperatures of the circulating fluid at the inlet and outlet of the heat exchanger (not shown here) shows that the outlet temperature reaches steady state conditions within 2 days, indicating a nearly constant thermal storage capacity of the test soil. Temperature profiles for sensors installed in the soil showed that a steady state condition for soil temperature was established faster compared to the outlet temperature (i.e. less than 2 days). Similar behavior was observed in the other three experiments.

Profiles of temperature in the soil for EX-2 at steady state conditions are shown in Figure 3(a). Because of symmetry, the results from only half of the sensors are shown. The closer the sensor is located to the heat plate at the edge of the container, the higher the observed temperature. The thermal gradient dissipates towards the centerline of the tank, resulting in a concavity of the temperature profile and decrease in soil temperature. This, in part, is due to heat loss out the sides of the tank as well as heat loss due to the energy required to change liquid water to water vapor, i.e., evaporation (discussed later). Temperature trends throughout the depth of the tank can also be inferred from the figure; the temperature increases with depth in the tank. This can be explained by the relationship between λ and S. The bottom row of sensors is located in the saturated region ($S \approx 1$) while the degree of saturation decreases with height above the saturated region. Typically, as degree of saturation increases, the apparent thermal conductivity also increases according to the relationships shown in Figure 1. Partially wet soil can be considered as a composite mixture of water, air and soil grains (quartz mineral for the sands under investigation). Thermal conductivity of water, dry air, and quartz mineral are typically

0.58 (at 20°C), 0.024 (at 20°C), and 6.15-11.3 $W.m^{-1}K^{-1}$ (Bristow 2002), respectively. Therefore, the λ of partially wet soil as a mixture is a function of water and air content. The results suggest that availability of moisture and distance from the heat source are two important factors, contributing to the temperature variation in the soil. Figure 3(b) also shows the temperature variation with time in sensors located along transects A and B. As shown in the figure, steady state temperature is reached after about 1 day.

Similar to the results from EX-2 shown in Figure 3(b), the temperatures for EX1, 3 and 4 also reached steady state condition in approximately less than 2 days (not shown here). Trends for temperature change throughout the soil profile as well as with distance from the heat plates were consistent for all experiments. Nonetheless, the observed steady state values of temperature were different for each soil type, although the temperature of the inlet fluid was maintained equal to 60^{o}C. It is difficult to compare the temperature distribution in all experiments since the ambient condition was slightly different for each experiment specifically in EX-2. However, it is obvious from the data that a higher temperature for EX4 was observed throughout the soil tank. The increase in temperature for EX4 compared to that of other three experiments is most notably due to differences in soil porosity which can play an important role in thermal conduction through increasing direct inter-particle contact. The C7F3 soil type has a lower porosity compared to the other soils ($\emptyset$ = 0.245 to 0.318, 0.317 and 0.327) resulting in more soil grain contacts and hence a higher thermal conductivity for all saturation conditions. It should be mentioned that it is quite impossible to quantify the contribution of different heat transfer processes (i.e., conduction, convection and latent heat) for current experiment using the experimental data. Final steady state temperature distributions for all the experiments represent a non-linear trend (not shown here) similar to Figure 3(a). This non-linear behavior is in general agreement with previous studies (e.g. Cassel et al., 1969). One possible reason for this behavior can be the heat loss through the surface of the tank.

[Figure 3 here]

3.2 Saturation behavior

Experimental measurements of the degree of saturation as a function of time for EX-2 on two vertical transects (Transects A and B in Figure 2) are plotted in Figure 4. In general, the degree of saturation appears to exhibit more dynamic behavior compared to the temperature data shown in Figure 3(b). A drying effect can be easily seen in the data shown in Figure 4 at the locations of the sensors located close to the heat plate (transect B or sensor locations 1, 8, and 15). Along transect B, the drying rate decreases with distance from soil surface (i.e. in the saturated region where moisture availability increases). Dependency of the moisture distribution pattern on initial water conditions is highlighted in Bear et al. (1991). They showed that the distribution in volumetric water content in unsaturated soils subject to high heat gradients is dependent on the initial conditions. They mentioned that for each soil type, there is a critical value for initial degree of saturation, such that for the initial degree of saturations below this value, a significant drying will occur in the vicinity of hot boundaries. It can be theoretically shown that for sufficient water contents, the liquid water and water vapor transfer processes in presence of thermal and hydraulic head gradients in the system are less likely to reach equilibrium and consequently a continuous circulation of the moisture is expected (Gurr et al., 1952). However, in this experiment, the initial water content is not high enough to establish a continuous moisture circulation and therefore, a steady state moisture distribution pattern was established as seen in the nearly constant drying front close to the heat plates (Transect B).

[Figure 4 here]

Based on the theory of coupled heat and mass transfer, it is expected that the liquid water would move from bottom part of the tank (lower capillary pressure) towards the soil surface (higher capillary pressure) due to suction and from top to bottom due to gravity. It would also move from middle parts of the tank towards the heat plates in horizontal direction. Moreover, it is expected that water vapor would transfer from the soil closer to the heat plates to the middle of the tank. The vapor transfer could also occur from the bottom part of the tank toward soil surface since the temperature increases as distance from soil surface increases. In the experiments, a drying effect was observed on both sides of the container, and the degree of saturation increased in the middle of the tank. The results for the changes in degree of saturation along transect A provide experimental evidence for thermally induced flow in the system. An increasing trend in degree of saturation over time for the middle and top sensor (sensor #11 and #4) is an indication of moisture flow towards middle region of the tank. The combined effect of abovementioned transfer processes shows that a greater amount of moisture flow occurs most likely due to vapor transfer in both directions than liquid water transfer which is later confirmed by modeling results (see section 5.2).

The rate of moisture flow decreases closer to the soil surface, as reflected in the slightly steeper change in sensor #11 readings compared to sensor #4 throughout the experiment. The bottom sensor (sensor #18) along transect A shows a decreasing trend in the degree of saturation. Since the tank is connected to the constant head devices at the sides of the container, the moisture loss due to thermally induced flow should be compensated with water supplied by the constant head devices. Nevertheless, the rates of water loss and supply are not equal, potentially due to poor hydraulic connection in fine-grained soils such as #30/40 or #50/70 which led to have a decreasing trend of moisture profile in vicinity of sensor #18. This trend for sensor #18 is not seen in EX-1 (coarser #12/20 sand) where the hydraulic connection was better established.

An increase in the degree of saturation along transect A occurred in all of the experiments (not shown here). However, the rate of increase is different in each experiment due to the different hydraulic and thermal properties of the sands. In EX-1 and EX-2 in which relatively coarse-grained soils were used in the test tank, the rate of increase in the degree of saturation is similar. The lowest increase in degree of saturation was observed in EX-3 in which a uniform, fine sand was used. The greatest increase in the degree of saturation occurred in EX-4, which included a mixed sand. This is in part due to higher thermal gradients which results in higher moisture flow in the system as will be further discussed in section 5.4. This may indicate that mixed sand provides better conditions for moisture flow. Degree of saturation at the locations of sensors 7 and 14 along with the heat plate and visual observations of the drying front propagation reveal that a drying front was less prominent in EX-3 and EX-4 than in the EX-1 and EX-2, which involved coarse-grained soils. This observation is in agreement with the findings of Bear et al. (1991).

3.3 Thermal properties

In-situ measurements of thermal properties of soil permit comparison between the results from the experiments with the λ-S-T relationship to that of separate Tempe cell experiments using the same soils and packing conditions (Smits et al., 2010, 2013). In addition, in-situ measurements allowed us to experimentally capture the effects of coupled mass and heat transfer on thermal properties. The SH-1 sensor location was selected to allow for variation in degree of saturation and temperature over time.

Time series of the measured values of λ and α are shown in Figure 5, along with the values of temperature and degree of saturation in the vicinity of SH-1 sensor. After an initial decrease which is possibly due to a small amount of drainage of the system in initial stages of the experiment, λ and α both increased over the course of the experiment. This behavior is mainly due to the increase in degree of saturation at the same location. Although temperature also increased at the location over time, the rise in temperature had a minimal effect on the increase in soil thermal properties.

Previous studies demonstrated that an increase in S results in an increase in λ and α (e.g., Smits et al., 2013). In addition, λ and α increase with an increase in temperature, mainly due to the transfer of latent heat in soil, thus increasing the apparent thermal conductivity (e.g. Philip and de Vries, 1957; Momose and Kasubuchi, 2002; Smits et al., 2013). According to the experimental studies by Smits et al. (2013) on the same #30/40 sand, at intermediate saturations (~0.1-0.6), λ and α increase at temperatures above 50 ^{o}C, with the maximum enhancement near the residual degree of saturation for each sand (S = 9%). For high and near-zero degree of saturation, such enhancement was insignificant. At temperatures below 50 ^{o}C, Smits et al. (2013) found that there was not a measurable difference in λ with changes in temperature. For the experiment presented here, S values at the SH-1sensor location varied between 7-11% while the temperature varied between 20-30 ^{o}C, far too low values of temperature to have a measurable effect on the thermal properties. Therefore, it seems that the effect of temperature on λ is not considerable in the experimental conditions discussed here. On the other hand, as illustrated in Figure 5(b), the increasing trend for moisture in the vicinity of SH-1 sensor (both #3 and #4 sensors) seems to be the main cause of thermal conductivity enhancement over time. Comparing values of λ and α–S with those obtained in separate Tempe cell experiments conducted by Smits et al. (2013) show that the values match very well. This verification was needed to properly select the thermal property relationships for the numerical modeling (e.g. Campbell et al. relationship and parameters). The value of α shows similar behavior to λ, which implies that the volumetric heat capacity is not changing during the test because it is related to the thermal diffusivity as α=λ/C. Specifically, a nearly constant value of volumetric heat capacity of about 1.8 MJ.m-3.K was observed throughout the experiment.

The thermal properties of test soils at a single location (same as EX-2) with time were measured for all experiments (not shown here). The results for thermal properties and temperature change are similar in all of the experiments to those shown in detail for EX-2. Therefore, it appears that increase in degree of saturation is the main reason for enhancement of thermal properties for other experiments as well whereas temperature has minimal effect. In EX-4 with the mixed soil type, thermal conductivity and diffusivity are considerably higher than other soil types which are due to lower porosity and higher particle contacts. Although the rate of change is different for each experiment, an overall increasing trend was observed. Results also show similar trends for the thermal diffusivity as a function of time for all experiments at the same location. The similar trends for thermal conductivity and thermal diffusivity are due to nearly constant volumetric heat capacity observed for all experiments.

[Figure 5 here]

4 Numerical Model Formulations

The model used in this study is a modified version of the model described by Smits et al. (2011, 2012) which solves for heat, liquid water and water vapor flux and allows for non-equilibrium liquid/gas phase change. A detailed description of the model can be found in Smits et al. (2011); however, governing equations for mass and energy transport mechanisms as well as phase change are presented here.

4.1 Mass transport in porous medium

Darcy's law is used to model the non-isothermal, non-equilibrium, two phase flow in porous medium. In this regard, two different equations are defined for both the liquid and gas phases. The total gas phase is assumed to be ideal and a binary mixture of water vapor and air. These two equations are related by capillary pressure to form the following coupled differential equations (Bear, 1972):

$$\emptyset \frac{dS_w}{dP_c}\frac{\partial \rho_w P_c}{\partial t} + \nabla.\left(\frac{-\rho_w k_{rw} k_{int}}{\mu_w}(\nabla P_w + \rho_w g)\right) = -f_{vw} \quad (1)$$

$$\emptyset \frac{dS_a}{dP_c}\frac{\partial \rho_a P_c}{\partial t} + \nabla.\left(\frac{-\rho_a k_{ra} k_{int}}{\mu_a}(\nabla P_g + \rho_a g)\right) = f_{vw} \quad (2)$$

Where $\emptyset$ is the total porosity of soil, S_w and S_a are water and air degree of saturation (dimensionless), $\rho_w(kg.m^{-3})$, $\mu_w(Pa.s)$, ρ_a, μ_a are the density and dynamic viscosity of water and air respectively, P_c (Pa) is the capillary pressure in porous medium ($P_c = P_g - P_w$), k_{int} is the intrinsic permeability of soil (m^2), k_{rw} (dimensionless) and k_{ra} are the relative permeability of water and air respectively, g is the gravitational acceleration ($m^2.s^{-1}$) and f_{vw} ($kg.m^{-3}s^{-1}$) is the non-equilibrium phase change rate between water and its vapor which is a result of evaporation or condensation in the system. To calculate the unknown water and gas phase pressure (P_w, P_g), equations (1) and (2) are solved simultaneously. The model of van Genuchten (1980) is used to describe the WRC in this study and the relative permeability values for water and gas (k_{rw} and k_{ra}) were obtained by utilizing the van Genuchten-Mualem model (van Genuchten, 1980). Since the temperature considerably changes in the system, the P_c-S_w relationship requires modifications to account for the effect of temperature changes. Changes in the temperature can cause fluctuations in the surface tension (Assouline, 2006). Therefore, the P_c-S_w relationship measured in the room temperature can be modified by substituting the relationship $P_c(T) = P_c(T_{ref})\sigma(T)/\sigma(T_{ref})$ in the P_c -S_w relationship where T_{ref} is the reference temperature at which the original P_c-S_w relationship was measured. Previous studies have shown that classical models for WRC as the van Genuchten model commonly fails to describe the WRC well enough at low water contents (e.g., Ross et al., 1991). This inaccuracy can be even amplified at higher temperatures when water content is less than residual water content. Based on the work of She and Sleep (1998), the residual water content is assumed to change linearly as a function of temperature, as follows:

$$\theta_r(T) = \theta_r(293\text{ K})[1 - c(T - 293\text{ K})] \quad (3)$$

where c is a fitting parameter (She and Sleep, 1998).

4.2 Phase change under non-equilibrium conditions

In traditional liquid-gas phase change models, phase change between the liquid and vapor phases is often evaluated based on the assumption of equilibrium; evaporation or condensation behavior is often considered as an instantaneous process (e.g. Philips and de Vries, 1957; Bear et al., 1991). In modeling efforts based on the equilibrium assumption, the equilibrium vapor density is determined by Kelvin's equation. Kelvin's equation can describe the equilibrium condition between the relative humidity and capillary pressure in pore space (e.g., Lu and Likos, 2004):

$$\ln\left(\frac{\rho_{veq}}{\rho_{vs}}\right) = \frac{P_c V_m}{RT} \quad (4)$$

where ρ_{vs} ($kg.m^{-3}$) is the saturated vapor density, V_m is the molar volume of water (M_w / ρ_w), R is the universal gas constant ($J.mol^{-1}.K^{-1}$) and T (K) is the temperature. Using Kelvin's equation, one can readily find the relationship between vapor densities for both equilibrium and saturated conditions. The saturated vapor density changes with temperature and can be estimated using the empirical relationship of Campbell (1985), given as follows:

$$\rho_{vs} = \exp(31.37 - 6014.79T^{-1} - 7.92 \times 10^{-3}T)\,/T \times 10^{-3} \tag{5}$$

Therefore, the equilibrium vapor density can be calculated by rearranging (4) and incorporating the value of ρ_{vs} from Equation 5:

$$\rho_{veq} = \rho_{vs}\exp\left(\frac{P_c V_m}{RT}\right) \tag{6}$$

In several studies, the assumption of equilibrium phase change is called into question (e.g., Bénet et al., 2009). The study carried out by Bénet et al. (2009) showed that the characteristic time associated with thermal equilibrium is much lower than the characteristic time associated with mass transfer. In a macroscopic model for liquid-gas phase change in hygroscopic porous media such as soil, phase change velocity is considerably influenced by hygroscopic effects of porous media (Cherblane et al., 2007). Since limited experimental data are available on the soil types that were used in our work, a method based on the difference between the vapor pressure in air and the equilibrium pressure at the water-gas interface was used (Zhang and Datta, 2004). In this approach the phase change rate is defined as:

$$f_{vw} = \frac{b(\theta_w - \theta_r)RT}{M_w}(\rho_{veq} - \rho_v) \tag{7}$$

where ρ_v (kg.m^{-3}) is the vapor density and b is defined as a fitting parameter that is assumed to be a function of soil properties. The value of b was fitted using experimental data obtained in this study for each soil type.

4.3 Heat transfer in porous medium

Conduction, convection and later heat transfer due to phase change are considered as three main heat transfer mechanisms in soil. We assumed local thermal equilibrium between the gas, liquid and solid phases. By taking averages at the scale of a representative elementary volume (REV), the energy equation can be applied for each phase separately. Under the assumption of local thermal equilibrium, energy equations for each phase are then combined to yield a general form of heat transfer equation for porous media, given as follows:

$$(\rho c_P)^* \frac{\partial T}{\partial t} + \nabla.\left((\rho c_P)_w u_w T) + (\rho c_P)_g u_g T\right)\right) - \nabla.(\lambda_t \nabla T) = -Lf_{vw} - Q_s \tag{8}$$

where c_P ($J.kg.K^{-1}$) is the heat capacity for the phase, u_w (ms^{-1}) and u_g are the liquid and gas velocities respectively, Lf_{vw} is the latent heat due to phase change, λ_t is the apparent thermal conductivity $(W.m^{-1}K^{-1})$ and $Q_s(J.m^{-3}.s^{-1})$ is the heat loss from the system. The value of Q_s can be estimated by incorporating Newton's law of cooling. The heat loss coefficient was defined based on knowledge of the thermal properties of the soil tank and surrounding air and the difference between the ambient room temperature and temperature of the soil tank (i.e., Plexiglas). The term $(\rho c_P)^*$ represents the effective heat capacity for all three phases and can be described by assuming that surface porosity is equal to the total porosity of porous media:

$$(\rho c_P)^* = (1 - \emptyset)(\rho c_P)_s + \emptyset(\rho c_P)_w + \emptyset(\rho c_P)_g \quad (9)$$

The thermal conductivity model of Campbell et al. (1994) was used in this study to estimate the apparent thermal conductivity (λ_t) as it considers the effect of changes in temperature and degree of saturation on the thermal conductivity of the soil and has shown to be effective compared to other models. In this model, the thermal conductivity of a mixture is considered as a weighted sum of thermal conductivities of components. Furthermore, since the system operating temperature is relatively high in the experiments, the physical properties of the different phases can be affected by temperature. In order to take these effects into account, the density and viscosity of water and air are treated as functions of the system temperature at each point.

5 Numerical simulation and comparison with experimental results

In this section, numerical model results are compared to experimental results to better understand any discrepancies between theory and experiments and the validity of the proposed model. First, to validate the proposed two-dimensional, non-isothermal, non-equilibrium model, numerical results for temperature and degree of saturation are compared with experimental results from EX1-4. Secondly, the numerical model correspond to EX-2 was considered to discuss effective processes and finally to perform several parametric studies in following sections.

The boundary conditions applied for mass and energy transfer are depicted in Figure 6. As seen from Figure 6(a), for liquid water and water vapor flow, Neumann boundary conditions (no mass flux) were assumed for all boundaries. Figure 6(b) presents applied boundary conditions for heat transfer in porous media. The Neumann boundary conditions were used in top and bottom insulated boundaries. However, for right and left boundaries, since constant temperature was applied, Dirichlet boundary conditions were chosen. Initial ambient temperature was considered as an initial temperature for the entire domain which was slightly different for each experiment. To establish the initial conditions of soil saturation, as mentioned earlier, constant hydraulic devices were used to create variable degree of saturation conditions throughout the domain.

To develop the numerical model, the porous media properties, initial and boundary conditions of the experimental case were implemented. The system of differential equations was then solved using the COMSOL Multiphysics software package. The domain was discretized by using 8909 triangular elements. Smaller boundary elements were used in the boundaries with constant temperature (heat plates) and bottom valves (connection to the constant hydraulic devices) as well.

[Figure 6 here]

5.1 Model verification with experimental results

Figure 7 shows the simulated vertical profiles of both temperature and degree of saturation compared with experimental data along transect A and B (see Figure 2) at times t=0 and 7 days. Although the numerical model captures the trends in the experimental data well, some discrepancies exist between experimental and numerical results which are statistically confirmed with the R^2 values (ranging from 0.660 to 0.907). Deviations between simulated and measured degrees of saturation and temperatures may, in part, be due the accuracy and resolution of the Dielectric sensors and thermistors compared to the model. The EC-5 soil moisture sensor, for example, has a sampling volume (i.e. the volume of soil around the sensor, within which a change in degree of saturation affects the sensor readings) of 18 cm^3 (Sakaki et al., 2008) while the numerical model predicts a degree of saturation value at an exact point, rather than a volume average. For the transect located close to the heat plate (transect B), the predicted and measured residual degree of saturation at t=7days did not agree well. The observed degrees of saturation at the location of sensors #1 and #15 were lower than the model predicted, demonstrating that the tank dried faster than the model predicted for these times. As discussed in the theory section, the effect of temperature on the WRC properties were accounted for using the She and Sleep (1998) modification of the van Genuchten model; this model could not capture the drying behavior for transect B where the temperature values were above 35 °C. Poor estimation of residual water content at the location of sensors #1 and #15 at t=7days could also be in part due to changes in soil water retention properties with changes in bulk density within the soil column (Assouline,

2006) as will be discussed later in section 5.5 as the constitutive relationship selected for the WRC.

A comparison between predicted and measured temperatures at different locations within the test tank along transects A and B is shown in Figures 7(c) and 7(d). Although the observed and modeled temperatures disagreed, the model captured the general trend (R^2 values ranging from 0.660 to 0.907). The deviations between simulated and measured temperatures may be, due to the accuracy and resolution of the temperature sensors compared to the model. The shape of the temperature profile is associated with the nonlinear distribution of the thermal properties associated with water redistribution in response to temperature gradients (Prunty and Horton, 1994), heat loss out of the sides of the soil tank, and differences in the degree of saturation through the depth of the tank. The heat loss was accounted for in the model based on knowledge of the temperature distribution out of the tank and thermal properties of the Plexiglas tank material. The additional heat loss due to the latent heat of evaporation was also taken into account in the model by the transfer of latent heat as a result of liquid water-water vapor phase change. The latent heat transfer is responsible for the S-shape curve (blue line) by maximizing the heat transfer close to the heat plates above the saturated zone. Errors associated with prediction of numerical models for temperature and degree of saturation distribution under non-isothermal conditions as opposed to isothermal conditions was also reported by Bach (1992). Bach (1992) showed that adjusting the temperature coefficient of the matric potential resulted in better agreement between measured and predicted values. Thus, a closer fit might be obtained by implementing more realistic relationships of effective parameters in WRC. Possible sources of error in both experimental data and modeling process will be further addressed in future studies.

[Figure 7 here]

To better understand the water vapor and liquid water movement throughout the domain over time, a comparison was made between the initial and final degree of saturation distribution in the domain. The simulated distribution of degree of saturation within the domain at the end of the experiment (t=7days) is shown in Figure 8(b). The gradient plot depicts the liquid water distribution while the arrows represent the water vapor flow. As expected, saturation decreased in the vicinity of the heat plates and a dry region developed at both sides of the tank, adjacent to the heat plates, which is in agreement with experimental observations discussed in previous sections. Water vapor flow is observed to flow from the sides of the tank toward the centerline, as expected. To investigate the degree of saturation and temperature trends in the middle of the tank, three points were considered, and the degree of saturation and temperature at these points as a function of time are plotted in Figure 8(c) and (d). It should be mentioned that the fluctuations in the temperature and degree of saturation plots are caused by ambient air fluctuations which were implemented as an input function to the model to account for heat loss. Consistent with the experimental results, the simulated degree of saturation profiles show a slight increase in both temperature and degree of saturation at all three points, demonstrating that the model captures the increasing degree of saturation trends well. Nonetheless, comparison of the trends in the degree of saturation values from the experiment and simulation indicate that although model captured the trends well, it underestimated the increasing rates.

The increase in degree of saturation in the middle regions of the tank as well as the trends in the velocity field for gas phase (shown by the arrows in Figure 8(b)) demonstrate the contribution of thermally induced vapor flow to the overall saturation movement as will be further discussed in section 5.4. The water vapor movement is highest close to the heat plates and decreases with distance from the centerline. This is because the water evaporates from the regions close to the heat plates and condenses as it reaches the relatively colder regions towards the centerline of the domain. This then results in an increase in soil degree of saturation toward the centerline of the tank (hence the increase in degree of saturation for points 1-3). It is important to note that although liquid water flow also contributes to overall moisture flow in the domain; its magnitude is smaller compared to vapor flow which is in part due to smaller percentage of saturated soil. Although degree of saturation increases in all three points, the rates of increase are different. For point #1 which is closer to the saturated soil, the increase rate (slope of gray trend-line) is slightly smaller compared to point #2 located above point #1 (hence a lower degree of saturation). This could, in part, be due to better connectivity of air-filled pores in dryer soil (point #2) which provides a better medium for vapor to flow. Since the water vapor transfers from both sides toward centerline, the rate of degree of saturation increase for both points #1 and #2 are larger than point #3.

The temperature trends for points 1-3 are shown in Figure 8(d). Consistent with experimental results, since point #3 is closer to the heat plate; the temperature was higher compared to points #1 and #2. In addition, point #1 has a higher temperature than point #2; this is due, in part, to the difference in degree of saturation and consequently differences in thermal properties (e.g. apparent thermal conductivities). For instance, the higher degree of saturation at point #1 than point #2, resulted in a higher thermal conductivity, thus a higher temperature was reached. As seen in the Figure 8(d), after an initial sharp increase in temperature, temperature remains almost constant for all three points. Similar behavior was observed in experimental results (Figure 5(b)).

[Figure 8 here]

5.2 The importance of conductive and convective heat fluxes

Surface plots of conductive and convective heat fluxes (i.e., heat transferred by liquid water and water vapor flow) within the domain are shown in Figures 9(a) and 9(b), respectively. The convective heat flux is considerably larger than conductive heat flux, demonstrating that the liquid water and water vapor flow have more of a contribution to the overall heat flux than the conductive fluxes. Cary (1965) also showed that most of the rise in net heat flux at higher average temperatures was due to latent heat transfer of vaporization. Based on surface integration values of the two components of the convective heat flux (i.e. liquid water and water vapor flux), liquid water flow contributes less to the overall convective flux (about 10% of total convective flux) as compared to the convective flux due to water vapor flow within the domain. This contribution will vary of course with soil degree of saturation; the percentage of liquid water flow is related to the percentage of saturated soil (around 25% of total soil volume for t=7 days).

Conductive heat flux is a function of the temperature gradient and apparent thermal conductivity of the soil. Since the moisture flow within the domain alters the apparent thermal conductivity, it is expected to indirectly affect the conductive heat transfer rate. The results in Figure 9(a) indicate that a higher conductive flux is observed in the saturated soil than in the unsaturated soil. This is partially due to the higher thermal conductivity of the saturated soil than the unsaturated soil (e.g., λ_{dry} vs. λ_{sat} values).

It is evident from Figure 9(b) that convective heat fluxes are higher in unsaturated regions close to the heat plates which are located just above saturated soil. This is likely due to the higher phase change rate from liquid water to water vapor at these locations and can be explained by relating the phase change rate to the degree of saturation of the soil. As discussed by Ruiz and Benet (2001), at low degrees of saturation the liquid/gas interfacial area increases resulting in more locations for phase change to occur and hence higher phase change rates. Close to the heat plates above the saturated zone, at t=7days, the soil is below the residual degree of saturation and phase change can occur readily. Although the same degree of saturation conditions exist in the middle of the tank and at same vertical distance, the regions with higher convective flux do not extent to the middle part of the tank due to smaller evaporation rate. Since the evaporation is directly related to the temperature, in colder regions in the middle of the tank the temperature is not high enough to trigger evaporation. These findings clearly show that in SBTES systems installed in vadose zone, depending on the initial and boundary conditions, the convective heat flux can have major contribution to overall heat transfer. Therefore, it should be considered in modeling and designing efforts.

[Figure 9 here]

5.3 Effect of convective heat flux on saturation and temperature distribution

The impact of convective heat flux on the temperature and degree of saturation was evaluated by comparing model results with and without including convective heat flux. In the case where convection was removed, conduction was the only mechanism for heat transfer. No considerable change in degree of saturation is observed in Figure 10(a) when only the heat transfer equation was modified. However, the impact of convective heat flux on temperature shown in Figure 10(b) indicates a greater effect. A temperature difference of almost 2 °C was observed in middle of the tank and the effect of convective heat flux on temperature rise increases with distance towards the heat plate. The temperature difference between the cases with and without convective heat flux highlights the importance of convective heat flux in obtaining more realistic temperature distribution in SBTES systems.

[Figure 10 here]

5.4 Effect of thermal and hydraulic gradients on moisture flow

Temperature and total hydraulic head (i.e., suction and gravity) gradients are two main driving mechanisms for coupled heat and mass flow in porous media. Thus, calculating the range of variation for these gradients is necessary to draw conclusions on the effect of each individual variable on heat and moisture movement. Simulated surface plots of temperature and hydraulic head gradients at t=7 days are depicted in Figure 11(a) and (b), respectively. As seen from Figure

11(a), the temperature gradient is highest close to the heat plates and decreases with distance towards the centerline. The decreasing trend is slightly different in the bottom region of tank where the soil is mostly saturated. As illustrated in Figure 11(b), the total hydraulic head gradient is considerably higher in the distinct boundary of the wetting front but it is negligible in rest of the domain (about 0.15 cm H_2O/cm). Cary (1965) experimentally studied the contribution of hydraulic head and thermal gradients to net moisture flow. Based on his studies with separate liquid and vapor flow components as well as flow due to thermal gradient and pressure difference, a temperature gradient of 0.5 ^{0}C cm^{-1} at a soil suction of 5 cm Hg (about the total hydraulic head range within wetting front in current study), caused a moisture movement as much as a soil suction of 2 cm H_2O/cm. Therefore by considering the magnitude of each gradient in this study, it appears that moisture flow is more influenced by thermal gradients than total hydraulic head gradients. Although the moisture flow and distribution in the soil does not

It is important to note that the hydraulic gradients may be more important than the thermal gradients at larger scales and at different initial degrees of saturation compared to this experimental study. However, as far as findings of current numerical simulations reveal, the thermal gradients should be taken into account to simulate moisture distribution when implementing field scale SBTES systems. Thermal and hydraulic gradients are closely coupled in SBTES systems; therefore it is critical to understand their relative importance for properly determining SBTES system behavior.

[Figure 11 here]

5.5 Effect of temperature correction on soil water retention

As mentioned in section 4.3, the WRC can be corrected to account for effects of temperature on the surface tension and residual degree of saturation (She and Sleep, 1998). These corrections were applied to consider the effect of temperature on the soil water retention function. To investigate the impact of these corrections on the model output, a simulation was performed with and without applying the temperature corrections to the WRC; results were compared to the base case scenario (EX-2) (with temperature corrections). The impact of the temperature correction is observed by looking at degree of saturation and temperature as a function of time in a sample point of the domain (point 2 in Figure 8(b) was selected here). As depicted in Figure 12(a), the model predicted higher values for both degree of saturation and temperature when no correction was applied to the WRC. For a constant capillary pressure, including the effect of higher temperature will result in a lower degree of saturation. This could be a main reason for the calculated degree of saturation level being lower when temperature is taken into account. Furthermore, as evident from Figure 12(a) without using a temperature correction for the WRC, fluctuations in ambient temperature do not affect the calculated degree of saturation values, resulting in a more consistent trend. It is important to highlight that in the original form of the van Genuchten model (i.e. no temperature correction); degree of saturation does not drop below the residual degree of saturation value. For this reason, although not shown here, the model failed to properly predict the drying behavior close to the heat plates when the effect of temperature on the WRC was not considered. In most of previous SBTES modeling efforts, there was no need to implement WRC in numerical models since the multiphase flow within the soil was not considered. However, for the models that incorporate non-isothermal multiphase flow, the proper correction for temperature in WRC should be considered.

[Figure 12 here]

5.6 Effect of porosity and saturated hydraulic conductivity

To examine the effect of porosity and hydraulic conductivity on degree of saturation and temperature, two sets of simulations were performed. In both sets, porosity and hydraulic conductivity values were changed by ±10% with respect to the base case values. Figure 13(a) shows the effect of porosity on the degree of saturation trend. Figure 13(c) and (d) shows the effect of saturated hydraulic conductivity on the degree of saturation and temperature respectively. As seen from the figure, hydraulic conductivity does not have a measurable effect on temperature and degree of saturation trends. At lower initial degree of saturations as in present study, saturated hydraulic conductivity is not as influential as, for example, WRC and relative permeability functions. The simulation clearly shows the importance of properly assigning porosity values to get more realistic degree of saturation distribution especially in field scale SBTES systems with nonhomogeneous domains (i.e., porosity can decrease with distance from ground surface). Therefore, a proper approach should be applied to account for porosity variability in the domain. On the other hand, in the SBTES systems installed in the vadose zone with lower degrees of saturation, the hydraulic conductivity of soil would not considerably affect the temperature and moisture distribution.

[Figure 13 here]

5.7 Effect of thermal conductivity

As discussed in the introduction, common practice in most previous studies related to SBTES systems is to assume constant thermal properties for soil. Although this assumption can be realistic in some cases, it is not accurate for modeling multiphase flow in unsaturated soil under non-isothermal conditions. The impact of assigning constant values for thermal conductivity in the numerical model was evaluated by running the model with two different constant thermal conductivities (λ_{sat} and λ_{dry}). Figure 14 presents the results of degree of saturation and temperature for each scenario as compared to the base case in which the Campbell model was used to estimate λ as a function of degree of saturation. As seen from Figure 14(b), higher temperatures were calculated when λ_{sat} was defined as a constant thermal conductivity throughout the domain. This is due to the increase in conductive heat transfer as λ increases. Inversely, λ_{dry} causes a decrease in conductive heat flux and consequently leads to lower temperatures in the system. The effect of this temperature change is then reflected in the degree of saturation profiles as seen in Figure 14(a). As discussed in section 5.5, the decrease in temperature can alter the WRC and therefore change the calculated degree of saturation values. For instance, as temperature decreases, degree of saturation increases for a constant capillary pressure. This is in general agreement with the degree of saturation trends in Figure 14(a). Results demonstrate the importance of properly assigning the thermal conductivity in designing and implementing any SBTES systems in vadose zone as the effect of this property is much larger than other thermal or hydraulic properties of the soil.

[Figure 14 here]

5.8 Numerical results for a natural soil: Bonny silt

Now that the model has been validated using experimental results, it is possible to evaluate the physics of coupled heat and mass transfer in soil layers that will likely be encountered in SBTES systems in the vadose zone. Accordingly, simulations with same assumptions and formulations were performed using the thermal and hydraulic properties of a natural soil named “Bonny Silt” (Dong et al., 2014). General properties of the soil are provided in Table 1. The same geometry for soil domain was considered to simulate three cases with different initial saturation conditions. In the first case, initial degree of saturation of approximately 19% was considered while in the second case, the initial variable degree of saturation was varied between 48% to about 51% and an almost saturated initial condition (89 %< S<100%) was considered in the third case. These simulations were aimed at investigating the effect of initial moisture condition on temperature and moisture transfer within the soil. The variation in initial degree of saturation is due to the approach used to create initial condition. An initial temperature of 21.3 °C was assumed for all simulations.

For all three cases, a vertical profile of initial and final values of degree of saturation and temperature along transect A are illustrated in Figure 15. This figure clearly shows that maximum change in degree of saturation and temperature occurs in case one (S=19%), while case three with higher initial degree of saturation level, exhibits minimum variation in both temperature and degree of saturation. These results therefore reveal that heat and mass transfer processes highly depend upon initial saturation conditions. To better illustrate the effect of convective heat flux on temperature distributions, the final temperature profiles were plotted with and without (green dotted line) taking the convective component of heat transfer into account. Figure 15(b) shows that convective heat flux has more contribution in soil with lower initial degree of saturation as opposed to higher initial degree of saturation (Figure 15(f)). As illustrations of Figure 15 reveal, there is a correlation between moisture variation and convective heat transfer. A comparison between temperature profiles for all three cases demonstrates that as initial degree of saturation of the soil increases the effect of convective heat transfer on temperature rise decreases while conduction becomes more significant. It can thus be suggested that for each soil type, there might be a critical degree of saturation in which overall heat transfer is maximum. Similarly as reported by Bear et al. (1991), there is also a critical degree of saturation (which depends on the soil type) that causes no considerable drying at the hot boundaries.

[Figure 15 here]

6 Conclusions

This paper reported a study where a two-dimensional, non-isothermal, non-equilibrium model for coupled heat and mass transfer processes was developed and evaluated using experimental data. The experimental and numerical results show that the hydraulic and thermal processes in unsaturated soil are coupled and therefore, their effect should be simultaneously analyzed in any SBTES system installed in vadose zone. Although limited, the experimental results for different soil types indicate that mixed soils with minimal porosity and varying grain size distribution would possibly lead to higher temperature gradients and consequently higher moisture flow in the system; therefore are suitable for SBTES systems. Furthermore, constant volumetric heat capacities for all studied sand types implies that non-isothermal conditions in similar unsaturated conditions may lead to a rate of heat injection/extraction, but will not change the overall amount of heat that can be stored.

For initial and boundary conditions assumed in this study, results indicate that convective heat flux is considerably larger than conductive heat flux, demonstrating the importance of including convective heat transfer in modeling of SBTES systems, especially in the unsaturated soils when water vapor phase is present. Returning to the concerns presented at the beginning of this study, it is possible to state that SBTES systems in vadose zone may have greater heat transfer capabilities due to effect of convective heat fluxes.

Analysis of thermal and hydraulic head gradients reveal that for the soil types, boundary conditions and initial conditions evaluated in this study, moisture flow (i.e., in terms of total flow in liquid and vapor phases) is influenced more by thermal gradients rather than total hydraulic head gradients. However this finding might not be valid for larger scales with different soil types and initial moisture contents. In larger scales, hydraulic gradients will be more important compared to smaller experimental scales such as current study.

The validated model provides a suitable tool to explore model sensitivity to different inputs and assumptions, including apparent thermal conductivity, soil water retention properties and porosity. It is therefore important to include more realistic equations/assumptions in defining apparent thermal conductivity (e.g. the effect of degree of saturation and temperature on soil thermal conductivity), the WRC (e.g., temperature effects) and porosity variation when modeling SBTES systems in unsaturated soils. The sensitivity analysis of validated model showed that traditional Van Genuchten model is not applicable in presence of high thermal gradient. Therefore, in order to consider the coupled hydraulic and thermal processes in SBTES systems, the effect of temperature should be considered in WRC. An implication of these findings is that SBTES systems in the vadose zone where unsaturated conditions are present should include variable thermal and hydraulic properties.

Numerical simulation of Bonny silt revealed that convective heat flux is not as pronounced in saturated soils than unsaturated soils, which indicates that SBTES systems in saturated soil will not have a change in the rate of heat injection/extraction during the inject/extraction process. Nonetheless, they may still be affected by buoyancy changes due to changes in temperature of the fluid. Furthermore, the simulations for Bonny silt highlight the importance of initial degree of saturation on convective heat flux. In general, for any specific SBTES system, there is possibly an initial degree of saturation in which convective heat transfer and consequently overall heat transfer is maximized.

This research demonstrates the need for further experimental and theoretical study on SBTES system behavior in three dimensional and field scales, the effect of boundary conditions (e.g. heat source temperature, distance of constant temperature boundaries), initial moisture conditions and incorporating different formulations/assumptions to define soil thermal and hydraulic properties. The findings of this study also indicate that SBTES system efficiency can be affected in different ways by coupled heat and mass transfer processes in the vadose zone. Further research is needed to evaluate how these processes can be exploited, specifically focusing on the impact of these mechanisms on the injection/extraction schemes and the long-term efficiency. It is also important to note that in natural soils, solute transport effects may impact the heat transfer process at hot boundaries. Drying out effect can increase the solute concentration close to the hot boundaries leading to lower equilibrium vapor pressure. Convective, dispersive and diffusive solute transport as well as osmotic effects can then develop as a result of variation in equilibrium vapor pressure (Bear et al., 1991). Hence, more experimental and theoretical investigations are required to better understand the effect of more complex processes such as solute transport on coupled heat and moisture transfer in natural soil under non-isothermal conditions.

Acknowledgments

This research was funded by National Science Foundation (NSF) Sustainable Energy Pathways (SEP) Collaborative, Award Number CMMI-1230544. The content is solely the responsibility of the authors and does not necessarily represent the official views of the National Science Foundation (NSF).

References

Abu-Hamdeh, N.H., 2003. Thermal properties of soils as affected by density and water content. Biosysttems Engineering 86, 97–102.

Angelotti, A., Alberti, L., La Licata, I., Antelmi, M., 2014. Energy performance and thermal impact of a Borehole Heat Exchanger in a sandy aquifer: Influence of the groundwater velocity. Energy Conversion and Management 77, 700-708.

Assouline, S., 2006. Modeling the relationship between soil bulk density and the water retention curve. Vadose Zone Journal 5, 554–563.

Bach, L.B., 1992. Soil water movement in response to temperature gradients: experimental measurements and model evaluation. Soil Science Society of America journal 56, 37–46.

Bear, J., 1972. Dynamics of Fluids in Porous Media. Dover, Mineola, N.Y., 764 pp.

Bear, J., Bensabat, J., Nir, A., 1991. Heat and mass transfer in unsaturated porous media at a hot boundary: I. One-dimensional analytical model. Transport in Porous Media 6(3), 281-298.

Bénet, J.C., Lozano, A.L., Cherblanc, F. and Cousin, B., 2009. Phase change of water in a hygroscopic porous medium. phenomenological relation and experimental analysis for water in soil. Journal of Non-Equilibrium Thermodynamics 34, 133–153.

Bouyoucos, G.J., 1915. Effect of temperature on the movement of water vapor and capillary moisture in soils. Journal of agricultural research 5, 141-172.

Bristow K.L., 2002. Thermal conductivity. In: Dane J.H., Topp G.C. (eds): Methods of Soil Analysis. Soil Science Society of America, Inc., Madison, 1209–1226.

Campbell, G. S., 1985. Soil physics with BASIC: transport models for soil-plant systems, Elsevier, Amsterdam, New York.

Campbell, G.S., Jungbauer, J.D., Bidlake W.R. and Hungerford, R.D., 1994. Predicting the effect of temperature on soil thermal conductivity. Soil Science 158(5), 307-313.

Carslaw, H.S., Jaeger, J.C., 1946. Conduction of heat in solids. Oxford UK, Claremore Press.

Cary, J.W., 1965. Water flux in moist soil: Thermal versus suction gradients. Soil Science 100, 168-175.

Cassel, D. K., Nielsen, D. R. and Biggar, J. W., 1969. Soil-water movement in response to imposed temperature gradients. Soil Science Society American proceedings 33, 493–500.

Cherblanc, F., Lozano, A.L., Ouedraogo, F. and Bénet, J.C., 2007. Non-equilibrium liquid-gas phase change in hygroscopic porous media. In: European Drying Conference, Biarritz, France.

de Vries, D.A. 1963. Thermal properties of soils. In Physics of plant environment. Edited by W.R. van Wijk. North-Holland, Amsterdam.

Diao, N., Zeng, H., Fang, Z., 2004. Improvement in modeling of heat transfer in vertical ground heat exchangers. HVAC&R Research 10, 459–470.

Dong, Y., McCartney, J.S. and Lu, N., 2014. Critical review of thermal conductivity models for unsaturated soils. In review, Geotechnical and Geological Engineering.

Eskilson, P., 1987. Thermal Analysis of Heat Extraction Boreholes. Doctoral Thesis. Department of Mathematical Physics, University of Lund, Lund, Sweden, 264 pp.

Florides, G. and Kalogirou, S., 2007. Ground heat exchangers - A review of systems, models and applications. Renewable Energy 32(15), 2461-2478.

Gabrielsson, A., Bergdahl, U. and Moritz, L., 2000. Thermal energy storage in soils at temperatures reaching 90 degrees C. Journal of Solar Energy Engineering-Transactions of the Asme 122(1), 3-8.

Gurr, C.G., Marshall, T.J., Hutton, J.T., 1952. Movement of water in soil due to a temperature gradient. Soil Science 72(5), 335–344.

Hellstrom G., 1991. Ground heat storage: thermal analyses of duct storage systems. Doctoral Thesis. Department of Mathematical Physics, University of Lund, Sweden.

Hillel, D., 1998. Environmental Soil Physics. Academic Press, London, UK, p. 156. Irrometer Company Inc., 2009. WATERMARK Soil Moisture Sensor with Voltage Output– MODEL 200SS-V. #405. Riverside, CA. Available online at: http://www.irrometer.com/datasheets/405.pdf (verified 29 Sep. 2014).

Hughes, P., 2008. Geothermal (ground-source) heat pumps: Market status, barriers to adoption, and actions to overcome barriers. Oak Ridge National Laboratory, U.S. Department of Energy.

Ingersoll, L.R., Plass, H.J., 1948. Theory of the ground pipe source for the heat pump. ASHVE Trans 54, 339–48.

Johansen, O. 1975. Thermal conductivity of soils. Doctoral thesis. Norwegian University of Science and Technology, Trondheim (CRREL Draft Transl. 637, 1977).

Kizito, F., Campbell, C.S., Campbell, G.S., Cobos, D.R., Teare, B.L., Carter, B., Hopmans, J.W., 2008. Frequency, electrical conductivity and temperature analysis of a low-cost capacitance soil moisture sensor. Journal of Hydrology 352(3-4), 367-378.

Koltermann, C.E., and Gorelick, S.M., 1995. Fractional packing model for hydraulic conductivity derived from sediment mixtures. Water Resources Research 31(12), 3283-3297.

Lamarche, L., Kajl, S. and Beauchamp, B., 2010. A review of methods to evaluate borehole thermal resistances in geothermal heat-pump systems. Geothermics 39, 187–200.

Leong, W.H., Tarnawski, V.R., Aittomäki, A., 1998. Effect of soil type and moisture content on ground heat pump performance. International Journal of Refrigeration 21 (8), 595-606.

Lu N. and Likos, W.J., 2001. Unsaturated Soil Mechanics. John Wiley & Sons Inc., New York.

Maclean, D.J. and Gwatkin, P.M., 1946. Moisture movements occurring in soil due to the existence of a temperature gradient. Road Research Laboratory. Note No. RN/761.

McCartney, J.S., Ge, S., Reed, A., Lu, N., and Smits, K., 2013. Soil-borehole thermal energy storage systems for district heating. In: European Geothermal Congress, Pisa, 3-7 June, 10 p. CD-ROM.

Momose, T., and Kasubuchi, T., 2002. Effect of reduced air pressure on soil thermal conductivity over a wide range of water content and temperature. European Journal of Soil Science 53, 599–606.

Ohga, H. and Mikoda, K., 2001. Energy performance of borehole thermal energy systems. In: Proceeding of 7th International IBPSA Conference, pp. 1009−1016.

Pavlov, G.K. and Olesen, B.W., 2012. Thermal energy storage-A review of concepts and systems for heating and cooling applications in buildings: Part 1-Seasonal storage in the ground. Hvac&R Research 18(3), 515-538.

Philip, J.R., de Vries, D.A., 1957. Moisture movement in porous materials under temperature gradients. American Geophysical Union Trans. 38, 222-232.

Pinel, P., Cruickshank, C.A., Beausoleil-Morrison, I. and Wills, A., 2011. A review of available methods for seasonal storage of solar thermal energy in residential applications. Renewable & Sustainable Energy Reviews 15(7), 3341-3359.

Prunty, L. and Horton. R., 1994. Steady-state temperature distribution in nonisothermal, unsaturated closed soil cells, Soil Science Society of America Journal 58, 1358-1363.

Rees, S.J. and He, M., 2013. A three-dimensional numerical model of borehole heat exchanger heat transfer and fluid flow. Geothermics 46, 1-13.

Reuss, M., Beck, M. and Muller, J.P., 1997. Design of a seasonal thermal energy storage in the ground. Solar Energy 59, 247-257.

Ross, P. J., Williams, J. and Bristow K. L., 1991. Equation for extending water-retention curves to dryness. Soil Science Society of America journal 55, 923–927.

Ruelle, P., Laurent, J.P., 2008. CS616 (CS615) water content reflectometers. In: Evett, S.R., Heng, L.K., Moutonnet, P., Nguyen, M.L. (Eds.), Field Estimation of Soil Water Content: A Practical Guide to Methods, Instrumentation, and Sensor Technology. IAEA-TCS-30. International Atomic Energy Agency, Vienna, Austria, ISSN 1018- 5518.

Ruiz, T. and Benet, J.C., 2001. Phase Change in a heterogeneous medium: Comparison between the vaporization of water and heptane in an unsaturated soil at two temperatures. Transport in Porous Media 44, 337–353.

Sakaki, T., and Illangasekare, T.H., 2007. Comparison of height-averaged and point-measured capillary pressure-saturation relations for sands using a modified Tempe cell. Water Resources Research 43(12), W12502.

Sakaki, T., and Smits, K.M., 2014. Water retention properties of binary mixtures as affected by mixing fractions. Vadose Zone Journal. Submitted for Review.

Sakaki, T., Limsuwat, A., Smits, K.M. and Illangasekare, T.H., 2008. Empirical two-point α-mixing model for calibrating the ECH2O EC-5 soil moisture sensor in sands. Water Resources Research 44(4), W00D08.

She, H. Y. and Sleep, B. E., 1998. The effect of temperature on capillary pressure-saturation relationships for air-water and perchloroethylene-water systems. Water Resources Research 34(10), 2587–2597.

Shirazi, A.S. and Bernier, M., 2013. Thermal capacity effects in borehole ground heat exchangers. Energy and Buildings 67, 352-364.

Sibbitt, B., McClenahan, D., Djebbar, R., Thornton, J., Wong, B., Carriere, J. and Kokko, J., 2012. The Performance of a High Solar Fraction Seasonal Storage District Heating System - Five Years of Operation. Energy Procedia 30(0), 856-865.

Sibbitt, B., Onno, T., McClenahan, D., Thornton, J., Brunger, A., Kokko J., Wong. B., 2007. The Drake Landing Solar Community Project – Early Results. In: 2nd Canadian Solar Buildings Conference, Calgary (Alberta), Canada.

Smith, W. O., 1943. Thermal transfer of moisture in soils. American Geophysical Union Trans. 24(2), 511–524.

Smits, K. M., Cihan, A., Sakaki, T., and Illangasekare, T. H., 2011. Evaporation from soils under thermal boundary conditions: Experimental and modeling investigation to compare equilibrium and nonequilibrium-based approaches. Water Resources Research 47(5), W05540.

Smits, K.M., Cihan, A., Sakaki, T., Howington, S.E., Peters, J.F., and Illangasekare, T. H., 2012. Experimental and modeling investigation of soil moisture and thermal behavior in the vicinity of buried objects. IEEE Transactions on Geoscience and Remote sensing 51(5).

Smits, K.M., Sakaki, T., Howington, S.E., Peters, J.F., and Illangasekare, T. H., 2013. Temperature dependence of thermal properties of sands over a wide range of temperatures (30-70°C). Vadose Zone Journal 12(1).

Smits, K.M., Sakaki, T., Limsuwat, A. and Illangasekare, T. H., 2010. Thermal conductivity of sands under varying moisture and porosity in drainage-wetting cycles. Vadose Zone Journal 9(1), 172-180.

Tarnawski, V.R., Leong, W.H. and Bristow, K.L., 2000. Developing a temperature-dependent Kersten function for soil thermal conductivity. International Journal of Energy Research 24(15), 1335-1350.

Taylor, S.A. and Cavazza L., 1954.The Movement of soil moisture in response to temperature gradients. Soil Science Society of America journal 18, 351-358.

van Genuchten, M.T., 1980. A closed-form equation for predicting the hydraulic conductivity of unsaturated soils. Soil Science Society of America Journal 44(5), 892-897.

Varble, J.L., Chávez, J.L., 2011. Performance evaluation and calibration of soil water content and potential sensors for agricultural soils in eastern Colorado. Agricultural Water Management 101(1), 93-106.

Yadav, M.R., and Saxena. G.S., 1977. Thermal characteristics of the soils in relation to their physical parameters and moisture content. Journal of the Indian Society of Soil Science 25, 1-6.

Yang, H., Cui, P. and Fang, Z., 2010. Vertical-borehole ground-coupled heat pumps: A review of models and systems. Applied Energy 87(1), 16-27.

Zeng, H., Diao, N., Fang, Z., 2002. A Finite Line-Source Model for Boreholes in Geothermal Heat Exchangers. Heat Transfer—Asian Research 31 (7), 558-567.

Zeng, H., Diao, N., Fang, Z., 2003. Efficiency of vertical geothermal heat exchangers in ground source heat pump systems. Journal of Thermal Science 12(1), 77–81.

Zhang, J. and Datta, A.K., 2004. Some considerations in modeling of moisture transport in heating of hygroscopic materials. Drying Technology 22, 1983–2008.

Zhang, R., Lu, N., and Wu, Y.S., 2012. Efficiency of a Community-Scale Borehole Thermal Energy Storage. In: GeoCongress, pp. 4386-4395.

Table 1.Selected properties of test sands used in experiments

Experiments	Sand	d_{50} (mm)	Porosity	Residual Volumetric Water Content (m/m)	Saturated Hydraulic Conductivity, Ks, (m s^{-1})	van Genuchten (1980) WRC Model Parameters	
						Alpha (kPa^{-1})	n
EX-1	12/20	1.040	0.318	0.017	$3.76{\times}10^{-3}$	0.00816	12.69
EX-2	30/40	0.524	0.317	0.022	$1.06{\times}10^{-3}$	0.0060	17.81
EX-3	50/70	0.27	0.327	0.075	$2.90{\times}10^{-4}$	0.0026	29.76
EX-4	C7F3	-	0.245	0.010	$3.97{\times}10^{-4}$	0.0029	6.75
	Bonny silt	0.039	0.430	0.030	1.3E-6	0.0863	1.58

List of Figures

Figure 1. Thermal conductivity-degree of saturation and primary drainage capillary pressure- degree of saturation relationships measured at room temperature for all test soils.

Figure 2. Schematic of the test tank apparatus used in experiments discussed here (not to scale).

Figure 3. Steady state temperature (time = 7days) measured vertically from the middle of the soil tank toward the heat plate and (a) temperature variation with time along transects A and B for EX-2 (b).

Figure 4. Degree of Saturation with time for sensors located along transects A and B (EX-2).

Figure 5. Thermal properties of soil at the location of SH-1 sensor (a) in EX-2. Degree of Saturation and temperature profiles as a function of time for two adjacent sensors #4 and #3 for the same experiment (b). (M: Dielectric sensor, T: Temperature sensor)

Figure 6. Boundary conditions for two-dimensional configuration where T is temperature, P_w is water pressure, J_c is mass flux (liquid water or water vapor) and J_T is heat flux in the domain.

Figure 7. Simulated and observed degree of saturation and temperature profiles along transects A and B at 0 and 7 days. (a), (b) initial and final degree of saturation values and (c), (d) initial and final temperatures along transects A and B.

Figure 8. Simulated soil degree of saturation distribution (a) at t=0 and (b) t=7 days (arrows representing velocity field) within the tank. The lower part of the tank (white portion) with almost saturated soil is excluded from Figure 8 (a), 8(b) to better illustrate the soil degree of saturation differences throughout the unsaturated region. Points 1-3 were selected corresponding to locations for three points depicted in 8(b) to better illustrate the change in (c) degree of saturation and (d) temperature with time.

Figure 9. Surface plot of simulated conductive (a) and convective (b) heat flux. Arrows in Figure 9(b) show the velocity field for gas phase. (Units: W/m^2)

Figure 10. Effect of convective heat flux in (a) degree of saturation (b) temperature profile with time at point #2 as shown in Figure 8(b).

Figure 11. Simulated surface plots of (a) temperature gradient ($^{\circ}C/cm$) and (b) hydraulic head gradient (cm H_2O/cm) within the domain. Analysis of results demonstrates that thermal gradients have more contribution in moisture flow than total hydraulic head gradients.

Figure 12. Effect of temperature correction of the WRC on the predicted trends at point 2 in Figure 8(b): (a) degree of saturation (b) Temperature.

Figure 13. Effect of soil porosity (∅) in (a) degree of saturation (b) temperature with time and effect of saturated hydraulic conductivity (KH) in (c) degree of saturation (d) temperature at point #2 as shown in figure 8(b).

Figure 14. Effect of constant thermal conductivity in (a) degree of saturation (b) temperature profile with time at point #2 as shown in Figure 8(b).

Figure 15. Vertical profile of initial and final values for degree of saturation (a, c, e) and temperature (b, d, f) along transect A (Figure 2) for all three cases. Case 1: initial degree of saturation of approximately 19%, Case 2: 48 %< S<51%, Case 3: 89 %< S<100%

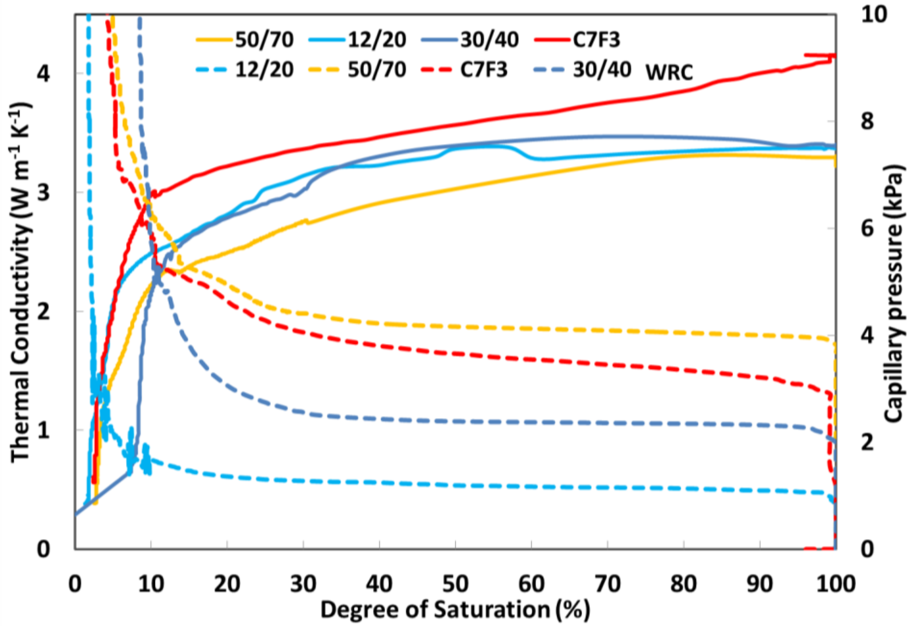

Figure 1. Thermal conductivity-degree of saturation and primary drainage capillary pressure- degree of saturation relationships measured at room temperature for all test soils.

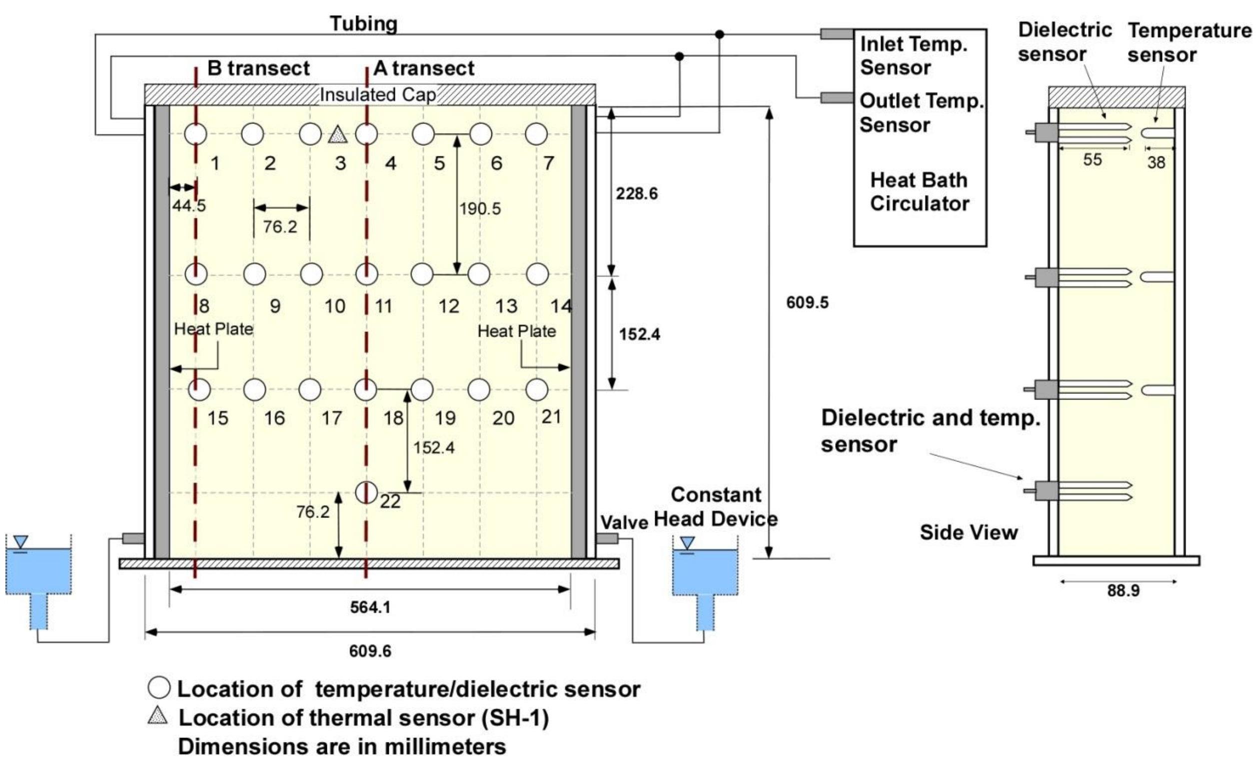

Figure 2. Schematic of the test tank apparatus used in experiments discussed here (not to scale).

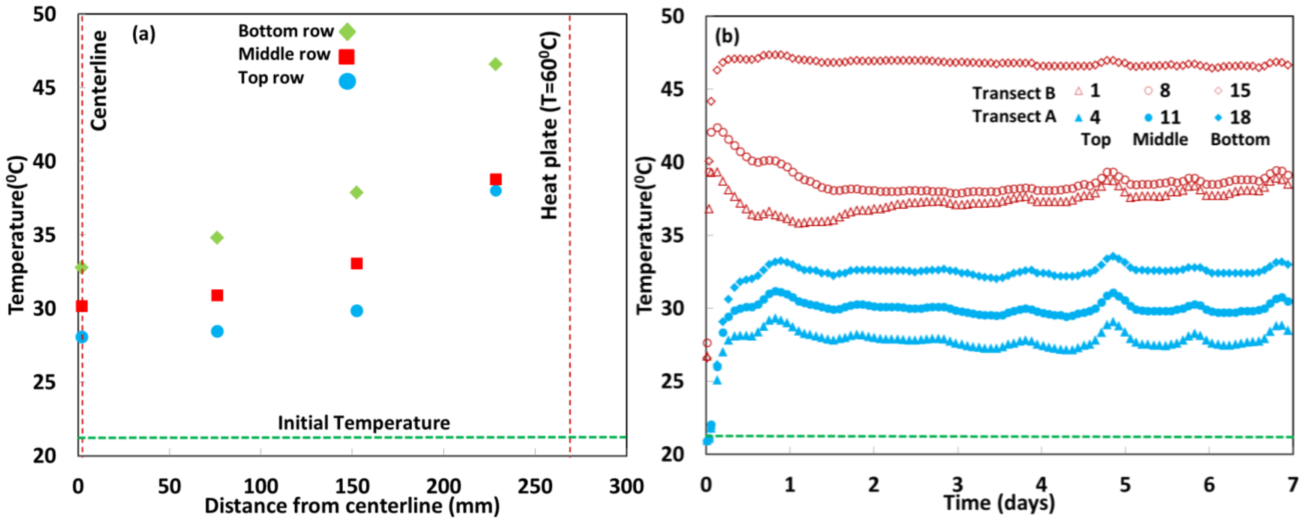

Figure 3. Steady state temperature (time = 7days) measured vertically from the middle of the soil tank toward the heat plate and (a) temperature variation with time along transects A and B for EX-2 (b).

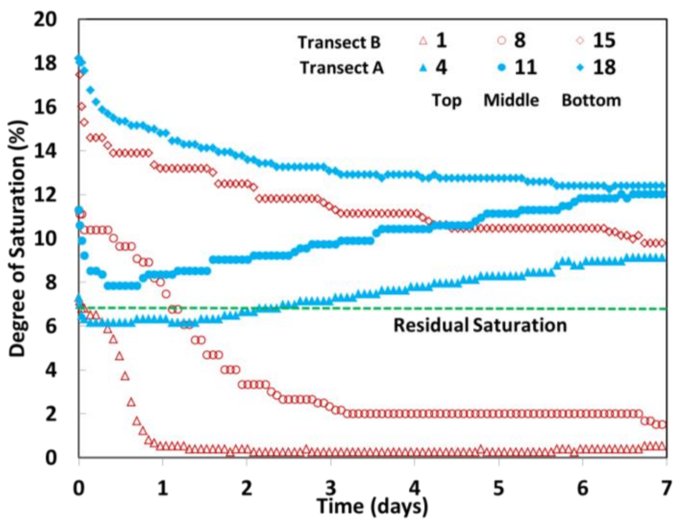

Figure 4. Degree of Saturation with time for sensors located along transects A and B (EX-2).

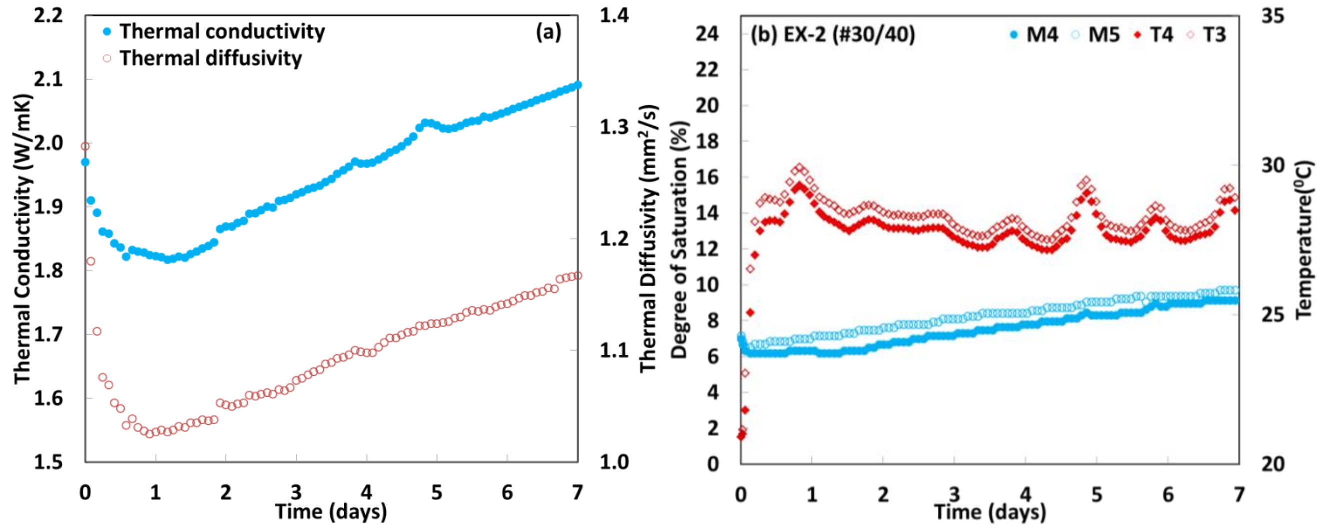

Figure 5. Thermal properties of soil at the location of SH-1 sensor (a) in EX-2. Degree of Saturation and temperature profiles as a function of time for two adjacent sensors #4 and #3 for the same experiment (b). (M: Dielectric sensor, T: Temperature sensor)

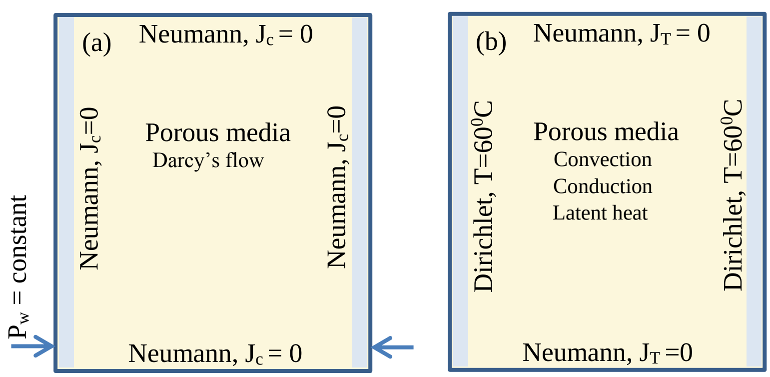

Figure 6. Boundary conditions for two-dimensional configuration where T is temperature, P_w is water pressure, J_c is mass flux (liquid water or water vapor) and J_T is heat flux in the domain.

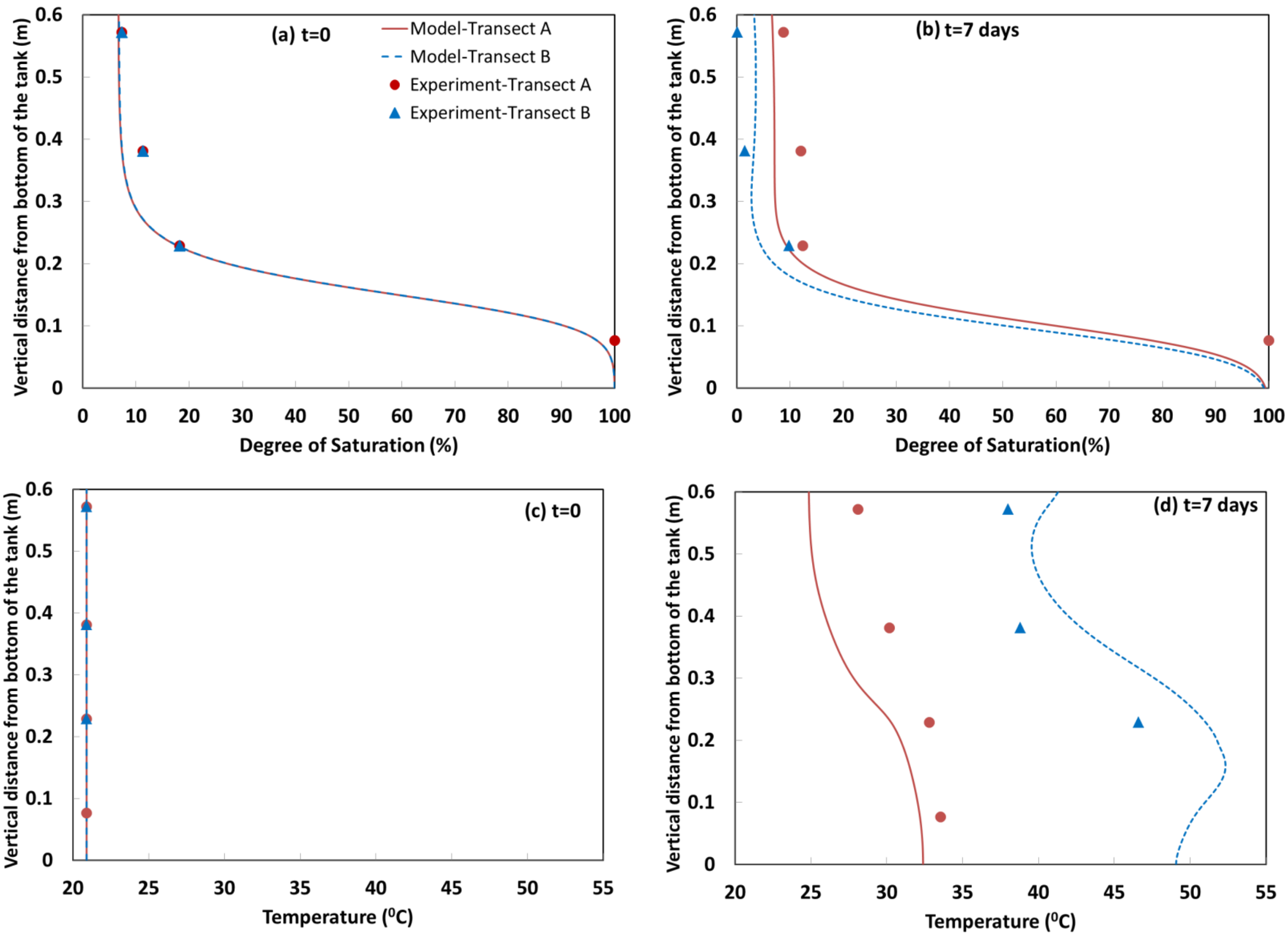

Figure 7. Simulated and observed degree of saturation and temperature profiles along transects A and B at 0 and 7 days. (a), (b) initial and final degree of saturation values and (c), (d) initial and final temperatures along transects A and B.

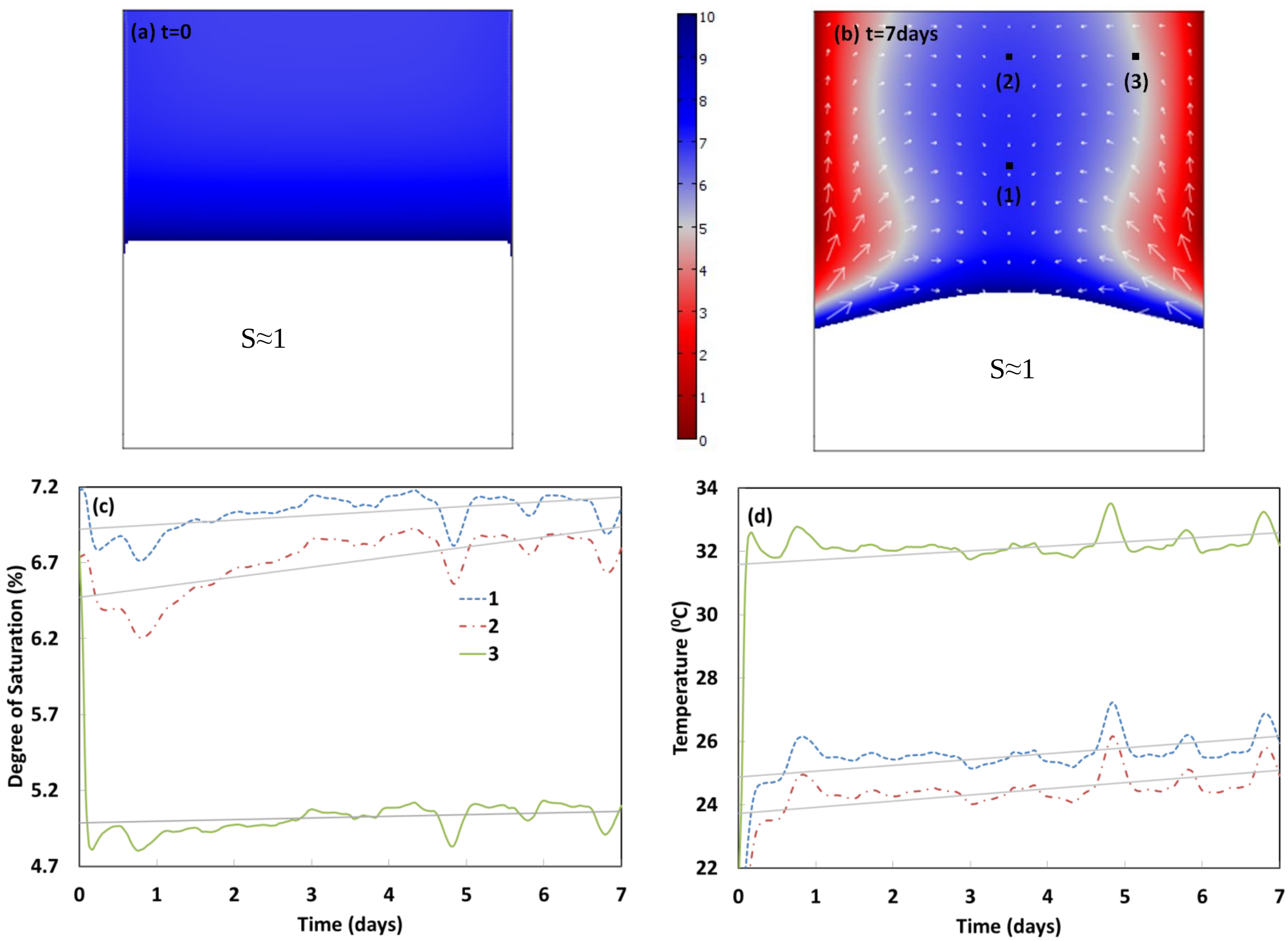

Figure 8. Simulated soil degree of saturation distribution (a) at t=0 and (b) t=7 days (arrows representing velocity field) within the tank. The lower part of the tank (white portion) with almost saturated soil is excluded from Figure 8 (a), 8(b) to better illustrate the soil degree of saturation differences throughout the unsaturated region. Points 1-3 were selected corresponding to locations for three points depicted in 8(b) to better illustrate the change in (c) degree of saturation and (d) temperature with time.

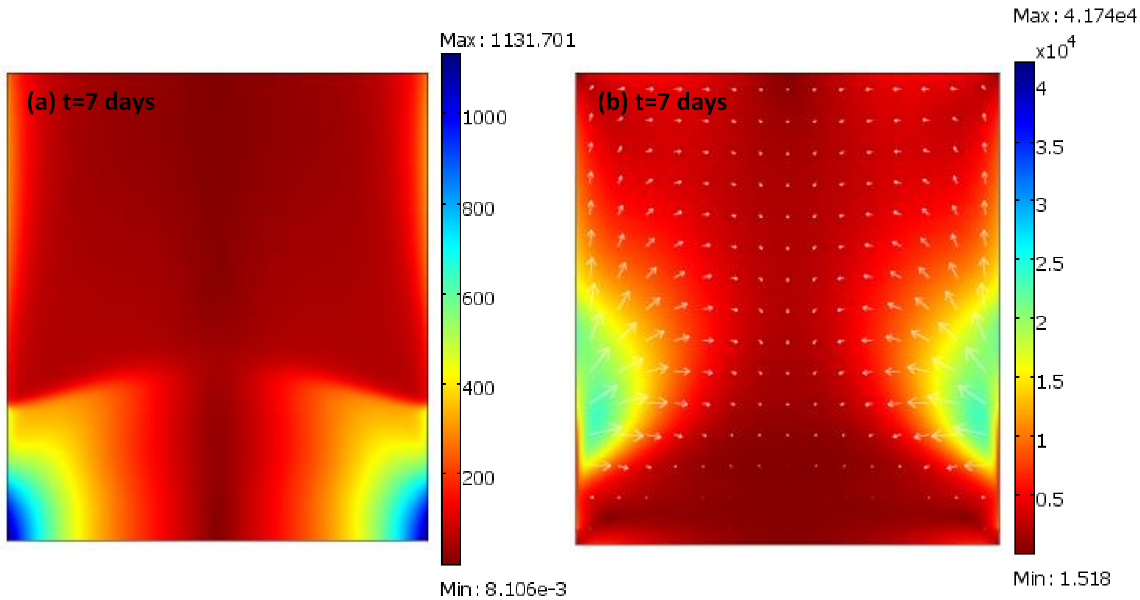

Figure 9. Surface plot of simulated conductive (a) and convective (b) heat flux. Arrows in Figure 9(b) show the velocity field for gas phase. (Units: W/m^2)

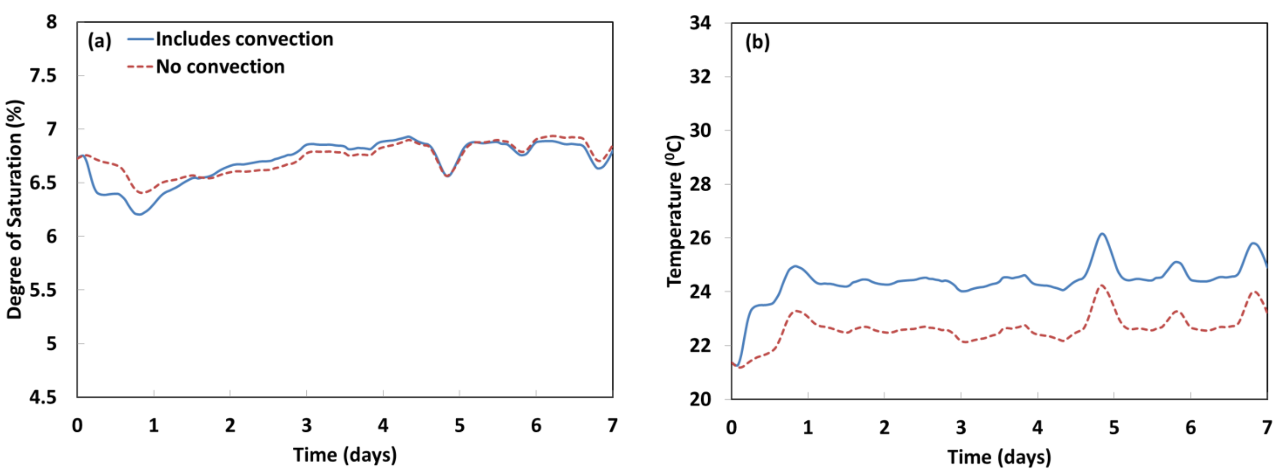

Figure 10. Effect of convective heat flux in (a) degree of saturation (b) temperature profile with time at point #2 as shown in Figure 8(b).

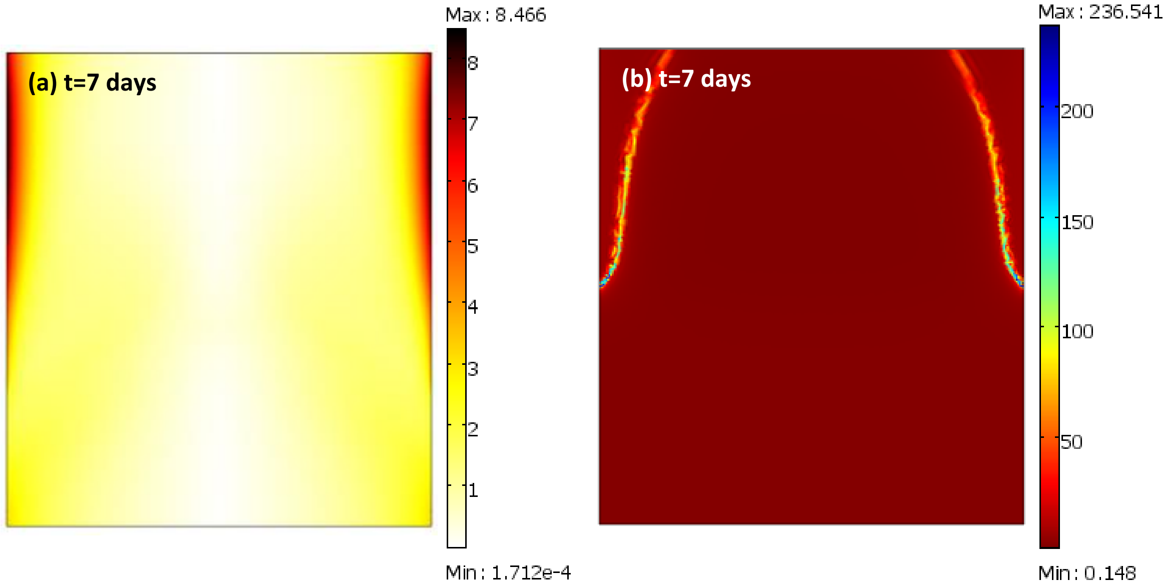

Figure 11. Simulated surface plots of (a) temperature gradient (°C/cm) and (b) hydraulic head gradient (cm H_2O/cm) within the domain. Analysis of results demonstrates that thermal gradients have more contribution in moisture flow than total hydraulic head gradients.

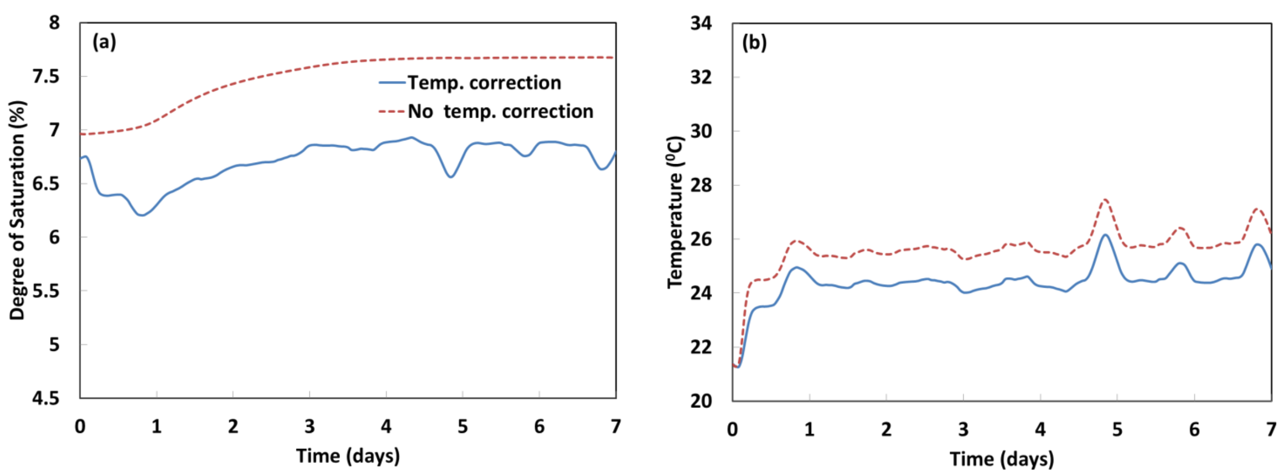

Figure 12. Effect of temperature correction of the WRC on the predicted trends at point 2 in Figure 8(b): (a) degree of saturation (b) Temperature.

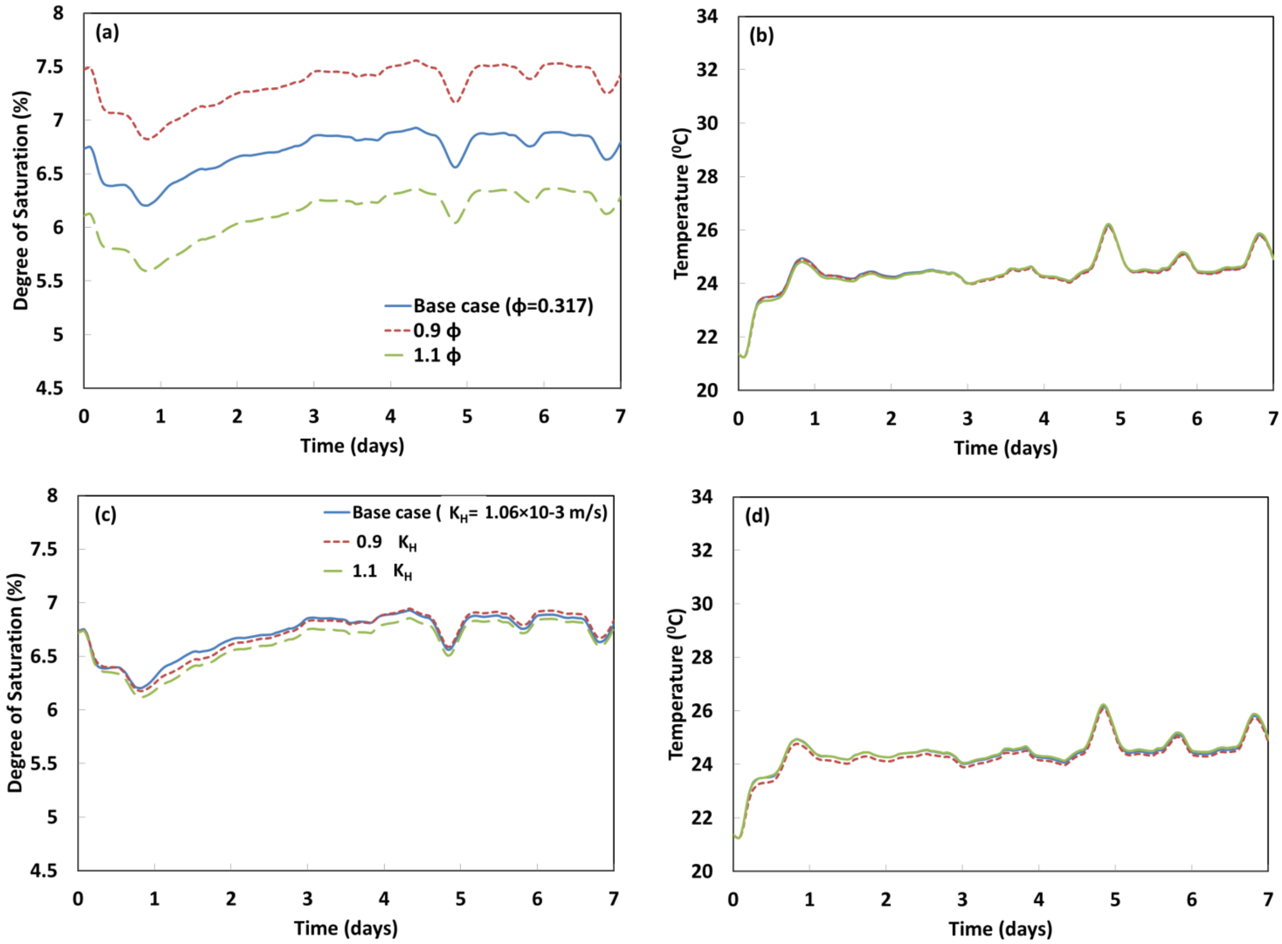

Figure 13. Effect of soil porosity (∅) in (a) degree of saturation (b) temperature with time and effect of saturated hydraulic conductivity (K_H) in (c) degree of saturation (d) temperature at point #2 as shown in figure 8(b).

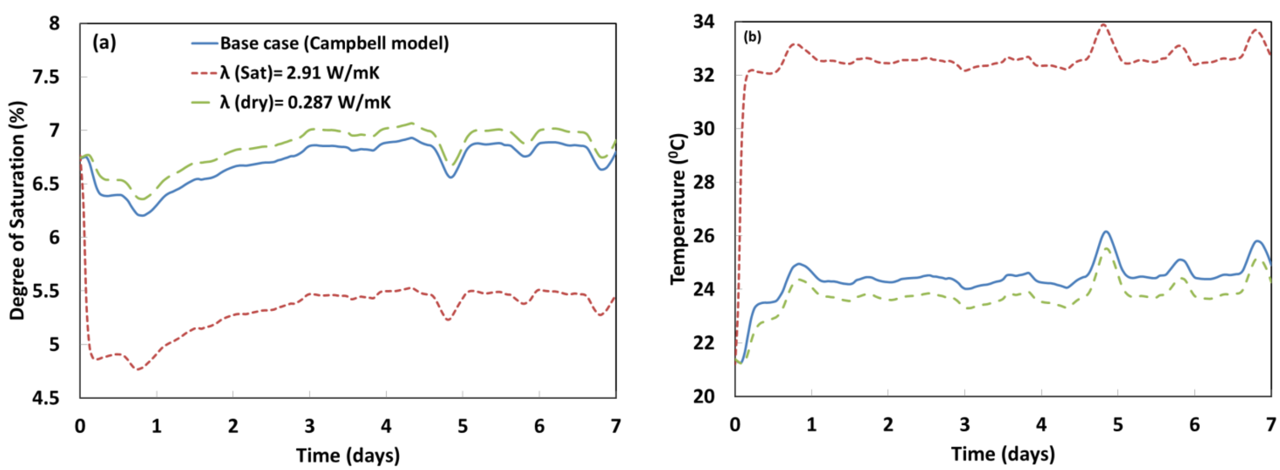

Figure 14. Effect of constant thermal conductivity in (a) degree of saturation (b) temperature profile with time at point #2 as shown in Figure 8(b).

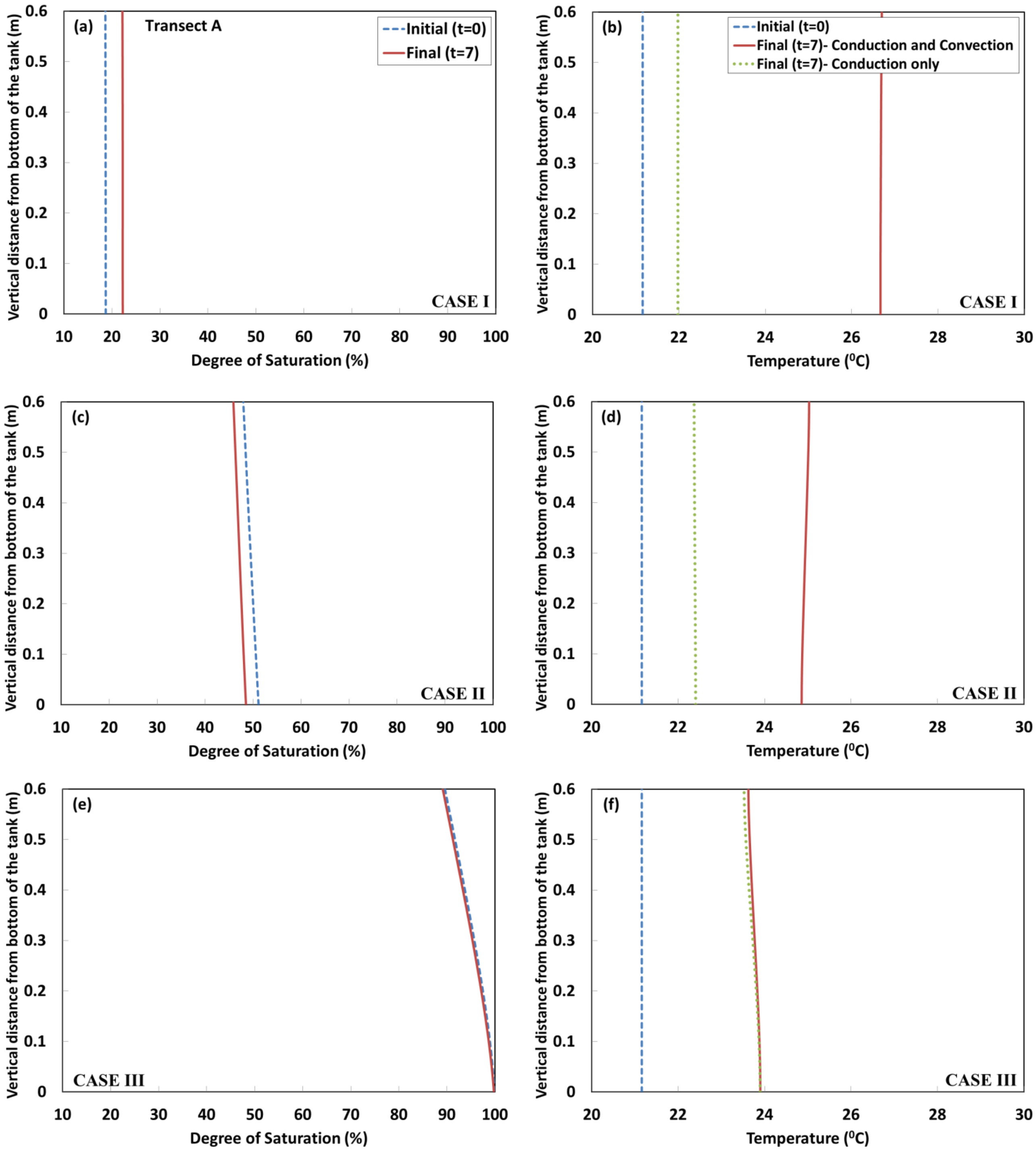

Figure 15. Vertical profile of initial and final values for degree of saturation (a, c, e) and temperature (b, d, f) along transect A (Figure 2) for all three cases. Case 1: initial degree of saturation of approximately 19%, Case 2: 48 %< S<51%, Case 3: 89 %< S<100%